Shape and Topology Optimization of Conformal Thermal Control Structures on Free-form Surfaces: A Dimension Reduction Level Set Method (DR-LSM)

Xiaoqiang Xu[a], Xianfeng David Gu[b,c], Shikui Chen[a,*]

[a]*Department of Mechanical Engineering, State University of New York at Stony Brook, Stony Brook, 11794, NY, USA*
[b]*Department of Computer Science, State University of New York at Stony Brook, Stony Brook, 11794, NY, USA*
[c]*Department of Applied Mathematics and Statistics, State University of New York at Stony Brook, Stony Brook, 11794, NY, USA*

Abstract

In this paper, the authors propose a dimension reduction level set method (DR-LSM) for shape and topology optimization of heat conduction problems on general free-form surfaces utilizing the conformal geometry theory. The original heat conduction optimization problem defined on a free-form surface embedded in the 3D space can be equivalently transferred and solved on a 2D parameter domain utilizing the conformal invariance of the Laplace equation along with the extended level set method (X-LSM). Reducing the dimension can not only significantly reduce the computational cost of finite element analysis but also overcome the hurdles of dynamic boundary evolution on free-form surfaces. The equivalence of this dimension reduction method rests on the fact that the covariant derivatives on the manifold can be represented by the Euclidean gradient operators multiplied by a scalar with the conformal mapping. The proposed method is applied to the design of conformal thermal control structures on free-form surfaces. Specifically, both the Hamilton-Jacobi equation and the heat equation, the two governing PDEs for boundary evolution and thermal conduction phenomena, are transformed from the manifold in 3D space to the 2D rectangular domain using conformal parameterization. The objective function, constraints, and the design velocity field are also computed equivalently with FEA on the 2D parameter domain with properly modified forms. The effectiveness and efficiency of the proposed method are systematically demonstrated through five numerical examples of heat conduction problems on the manifolds.

Keywords: Heat conduction, Conformal topology optimization, Conformal mapping, Conformal geometry theory, Dimension reduction level set method (DR-LSM)

1. Introduction

The increasing maturity of additive manufacturing has made possible the realization of structural designs with great geometrical complexity [1–3]. Powered by that, topology optimization,

*Corresponding author
Email address: Shikui.Chen@stonybrook.edu (Shikui Chen)

which seeks to find the optimal material distributions of the design for the desired performance, has also gained growing popularity [4, 5]. With the lifting of restrictions imposed by conventional manufacturing methods, researchers from topology optimization community now have more freedom and flexibility to optimize structures with multiple materials [6–10], at multiple scales [11–13], and in high conformality [14–16]. One way to ensure conformality requires solving topology optimization problems on thin-shell structures, commonly seen in, for instance, architectural design [17, 18], flexible electronics [19, 20], and aerospace engineering [21], to name a few. There have been many endeavors for thin-shell-based topology optimization. For example, some studies have [22–24] focused on structural optimization of composite laminates with varying fiber orientations. Using the homogenization method [25–27], Maute et al. [28] proposed an adaptive topology optimization scheme for shell structures, where maximum stiffness problems were tackled considering design model adaptivity. Ansola et al. [29] developed an automated approach for simultaneously optimizing the shape and topology of shell structures. A combined shape and reinforcement layout optimization of shell structure was subsequently investigated by Ansola et al. [30]. Clausen et al. [31] introduced a 3D topology optimization approach for shell structures with porous infill using solid isotropic material with penalization (SIMP) method. Tröff et al. [32] solved the topology optimization of ultra high-resolution shell structures using an efficient parallel multigrid preconditioner also in the SIMP framework. Density-based topology optimization methods are efficient to implement but subject to some numerical instabilities such as checkerboard pattern and mesh dependency [33]. The numerical instabilities can be effectively mitigated through filtering techniques [34, 35].

Mathematically, solving topology optimization problems on thin shells involves solving partial differential equations (PDEs) on surfaces. There are various approaches to solving surface variational problems. A common way is to use the finite element method [36, 37] directly on surfaces, which are usually discretized by surface triangulation. In some cases, the orthogonal projection will be required to ensure that the covariant derivatives are tangent to the surface [38]. Moreover, the discretization becomes nontrivial, and the computation of geometric quantities, such as surface normals or curvatures, poses a challenge in this method. Bartezzaghi et al. [39] dealt with the numerical approximation of high-order PDEs mainly on closed surfaces represented by B-splines or NURBS. Another popular approach is based on the level set method, where the original PDE is extended from the surface of interest to a narrow band [40] or 3D volume [41] such that the finite difference methods can be used for the numerical solution. The numerical implementation on the Cartesian grids makes this approach robust, accurate and efficient.

The variational problems or PDEs on surfaces can also be solved by parameterizing the surface onto a 2D parameter domain [42]. The extended level set method (X-LSM) proposed by Chen and Gu et al. [14, 43] has systematically investigated the structural shape and topology optimization on manifolds by integrating the conformal geometry theory [38, 44] into the level set framework. The key ingredient of the X-LSM is to conformally map the original manifold in 3D space to a 2D rectangular domain where the modified Hamilton-Jacobi equation is solved to evolve the structural boundaries. The rationality behind this modification lies in that the corresponding covariant derivatives on a surface can be represented by the Euclidean differential operators multiplied by a scaling factor based on the conformal parameterization [42]. This method elegantly extends the conventional level-set-based topology optimizations from the Euclidean space to manifolds.

Among the various topology optimization methods [25, 26, 45–50], the level set methods [46, 47] receive particular attention because of their clear boundary expression and flexibility in handling topological changes. The conventional level set based topology optimization algorithms typically work on fixed 2D or 3D grids, making them not well-suited for thin-shell structures. Based on X-LSM, a number of topology optimization problems on free-form surfaces were tackled, such as thermal problems [51, 52] and soft robots design problems [53–55]. Besides X-LSM, it is worth mentioning that Park et al. [56] proposed the adaptive inner-front (AIF) level set method for topology optimization of shell structures, where the set of transformation rules [57] were applied to convert the level set equation from Cartesian coordinates to curvilinear coordinates. Ho-Nguyen-Tan et al. [58] considered the minimization of both the compliance and stress of shell structures with trimmed quadrilateral shell meshes and the level set function defined directly on the surfaces.

In the original X-LSM [14], only the Hamilton-Jacobi equation that governs the boundary evolution, is transferred from the original manifold in 3D space to the mapped 2D domain. However, finite element analysis (FEA) is still performed on the freeform surface, which costs most of the computation time in topology optimization [59]. In this paper, we propose a Dimension Reduction Level Set Method (DR-LSM) for shape and topology optimization by incorporating the conformal geometry theory and X-LSM. Both the physics equation and the Hamiton-Jacobi equation, which govern the physics phenomena and the structural boundary evolution, are transferred and resolved from free-form surfaces in 3D space to 2D parameter domain. This dimension reduction formulation can significantly reduce the computational cost and algorithm complexity. The concept of the dimension reduction was first proved by Xu et al. [51], yet the computational saving capability of the DR-LSM was not systemically investigated. We apply the proposed DR-LSM to the design of conformal thermal control structures on free-form surfaces.

Efficient thermal management is critical to many engineering applications to maintain a moderate temperature field and extend the lifespan of the devices. Topology optimization has become a powerful tool for thermal structural design in recent years [60–64]. In particular, extensive studies have been carried out on topology optimization of heat conduction problems [65–70]. Previous attempts on pure heat conduction topology optimization problems mainly focused on planar 2D or solid 3D cases. For instance, Iga et al. [71] carried out topology optimization of thermal conductors considering the design-dependent effects using the homogenization method. Gersborg-Hansen et al. [72] used the solid isotropic material with penalization (SIMP) based topology optimization method and the finite volume method (FVM) to solve a 2D thermal conduction problem. Qing et al. [73] applied the evolutionary structural optimization (ESO) to effectively reduce the temperature at selected control points. Zhuang et al. [74] tackled the problem of level-set-based topology optimization on heat conduction under multiple load cases. Xia et al.[75] revisited the heat conduction topology optimization problems by combining the level set method with the bidirectional evolutionary optimization (BESO) approach to achieve better hole nucleation flexibility. Yamada et al. [76] studied a thermal diffusivity maximization problem with generic heat transfer boundaries under the level-set framework, where a fictitious interface energy was incorporated to regulate the topology optimization problem.

This study employs the proposed DR-LSM to address a minimum thermal compliance topology optimization problem on free-form surfaces. Under the conformal parameterization, the FEA is now conducted on the 2D parameter domain by solving a modified heat equation. The modified Hamilton-Jacobi equation is also solved on the 2D parameter domain to evolve the structural boundary. In addition, the related physics quantities, i.e., the objective function (thermal compliance), current volume and normal velocity field, will also be evaluated with properly modified forms on the 2D parameter domain. In this way, the 3D topology optimization problem is treated as a 2D problem. Several numerical examples are provided with comparisons with conventional X-LSM to demonstrate the effectiveness and advantages of the proposed DR-LSM.

1.1. Contributions

The major contribution of this work is to propose the dimension reduction level set method (DR-LSM) for shape and topology optimization on manifolds by incorporating the conformal geometry theory and the extended level set method (X-LSM). As a result, both the Hamilton-Jacobi equation and the thermal conduction equation, which are the two governing PDEs for the boundary evolution and the conductive heat transfer phenomena, are transformed from the manifold in 3D space to the 2D rectangular domain using conformal parameterization. The benefits of the proposed DR-LSM are as follows:

- **Rigorous:** the conformal geometry theory and the conventional level set based topology optimization method have solid mathematical foundations. The equivalence of this dimension reduction formulation is guaranteed.
- **Efficient:** By reducing the dimension from the manifold in 3D space to the 2D parameter domain, where well-developed numerical techniques can be employed, it can considerably reduce the computational costs.
- **Consistent:** the conformal parameterization is implemented to ensure the geometrical and physical consistency between the dimension-reduced problem and the original problem.
- **General:** the proposed method is applicable to free-form surfaces with different typologies and geometries. In addition, it can be extended to other physics problems other than heat conduction.

This paper is organized as follows: Section 2 will provide a theoretical background, including the conventional level-set method, the conformal geometry theory, the X-LSM, and the DR-LSM. The original problem formulation on the manifold will be detailed in Section 3, followed by the equivalent problem formulation on the 2D parameter domain in Section 4. The DR-LSM implementation algorithm is described in Section 5. Numerical examples will be presented in Section 6. Discussions and conclusions are given in Section 7.

2. Theoretical background

This section will provide theoretical background underlying the formulation of the proposed method.

2.1. Conventional level-set method

Initiated by Sethian and Wiegmann [77] and further completed by Wang [46] and Allaire [47], the level set approach has become a promising shape and topology optimization method, particularly for multimaterial and multiphysics problems. The level set method is able to generate and maintain a clear boundary during the optimization process. The structural boundary is implicitly represented as the zero contours of the one-higher dimensional level set function. This is a preferred property when a detailed description of the boundary is required. In the classical level set framework, the level set function is defined on a fixed background grid. The structural design is implicitly embedded in the level set function $\Phi(\mathbf{x},t)$ as follows:

$$\begin{cases} \Phi(\mathbf{x},t) > 0, & x \in \Omega, & \text{material} \\ \Phi(\mathbf{x},t) = 0, & x \in \partial\Omega, & \text{boundary} \\ \Phi(\mathbf{x},t) < 0, & x \in D\backslash\Omega, & \text{void} \end{cases} \tag{1}$$

The geometric level set model for a 2D structural boundary is shown in Figure 1. For the

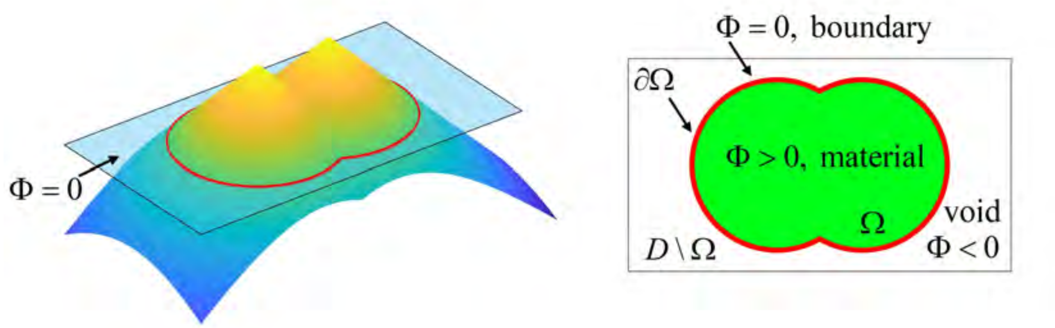

Figure 1: The level set representation of a 2D design

structural boundary, it always satisfies the equation $\Phi(\mathbf{x},t) = 0$. Differentiating both sides of the equation with respect to a pseudo time t leads to the Hamilton-Jacobi (H-J) equation [78]:

$$\frac{\partial\Phi(\mathbf{x},t)}{\partial t} - V_n \cdot |\nabla\Phi| = 0, \tag{2}$$

where $V_n = V \cdot (-\frac{\nabla\Phi}{|\nabla\Phi|}) = \frac{d\mathbf{x}}{dt} \cdot (-\frac{\nabla\Phi}{|\nabla\Phi|})$. The above H-J equation governs the dynamics of the structural boundary evolution. The shape sensitivity analysis can be conducted using the adjoint sensitivity method. The design velocity field is constructed case by case depending on specific optimization problems. It is worth mentioning that the conventional level set framework only works on 2D or 3D problems in the Euclidean space where the minimum distance between two points is the length of a line segment between them. The classical level set framework is unsuitable for topology optimization problems defined on general free-form surfaces.

2.2. Conformal geometry theory

In mathematics, conformal geometry studies the invariants under conformal transformations. Numerous theorems and algorithms have been developed in this area [44]. The plane-to-plane conformal mapping is governed by the Cauchy-Riemann equation and is one of the principal subjects of complex analysis. The surface-to-surface conformal mapping is described by the Dirac equation [79]. Our particular interest in this paper is the surface-to-plane conformal mapping, which is computed using Hamilton's Ricci flow theory [80]. Interested readers are referred to [81] for a detailed introduction to the Ricci flow.

2.2.1. *Conformal mapping of Riemannian surfaces*

Surface mapping will inevitably introduce distortions, such as distortions of distance, direction, shape, or area. Conformal mapping is essentially a function that preserves local angles but not necessarily lengths. It originates from differential geometry on the Riemannian manifold [44]. A visualization of the angle preservation property of conformal mapping is shown in Figure 2, where the infinitesimal circles on a surface are mapped to infinitesimal circles on a 2D disk.

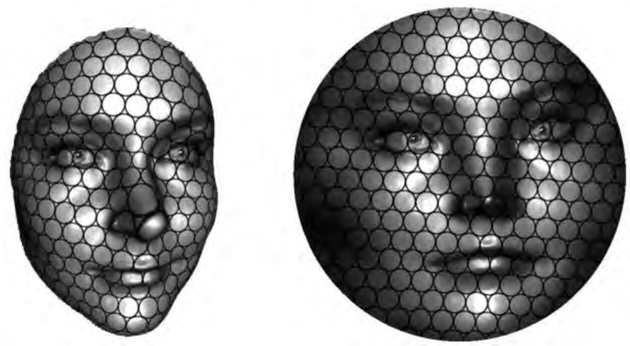

Figure 2: Conformal mapping from surface in 3D space to 2D disk [44]

Here, a strict mathematical definition of conformal mapping is provided. A Riemannian manifold M is normally accompanied with a Riemannian metric $\mathbf{g}$, which is essentially the inner product in each tangent space and allows us to measure lengths and angles. Suppose we are given two Riemannian manifolds (S, $\mathbf{g}$) and (T, $\mathbf{h}$). A smooth function $\varphi : S \to T$ is called *conformal* if the pull-back metric induced by φ differs a factor of scalar function with the original metric, i.e., $\varphi^{*}\mathbf{h} = e^{2\lambda}\mathbf{g}$, where $e^{2\lambda} : S \to \mathbb{R}$ is a scalar function called conformal factor. Although the conformal mapping will induce some area distortion, the distortion can be characterized by the conformal factor $e^{2\lambda}$. Geometrically, $e^{2\lambda}$ describes the area scaling effect, which varies from point to point. The factor e^{λ} will give the length scaling. To clearly show the geometric meaning of the conformal factor $e^{2\lambda}$, an example of conformal mapping is provided in Figure 3. Specifically, a semi-sphere with a uniform triangulation is conformally mapped to a rectangle on the 2D plane. The region with a denser 2D triangulation has a higher conformal factor value. This is consistent with the $e^{2\lambda}$ plot in Figure 3c.

2.2.2. *Differential operators on manifolds*

The conformal geometry theory has found many applications in the fields of engineering. Our particular interest is its application for solving PDEs on manifolds [38, 42]. With the conformal parameterization, the differential operators defined on the manifolds can be transferred into their Euclidean forms with a combination of the conformal factor $e^{2\lambda}$ describing the scaling effect of the conformal mapping.

Specifically, let M be a manifold in $\mathbb{R}^3$ and $\phi : \mathbb{R}^2 \to M$ be a global conformal parameterization of M. Suppose that the conformal factor of ϕ is $e^{2\lambda}$. A scalar function is defined on the manifold as $f : M \to \mathbb{R}$. With conformal parameterization, we can do calculus on surfaces in $\mathbb{R}^3$ as we do on planes in $\mathbb{R}^2$. We first define the partial derivative $D_{x_i}f$. On $\mathbb{R}^2$, the partial differential is usually defined by taking the limit, e.g., $\frac{\partial f}{\partial x} = lim_{\Delta x \to 0} \frac{f(x+\Delta x, y) - f(x,y)}{\Delta x}$. When defining $D_{x_i}f$ in the same manner, we must take into account the stretching effect of conformal mapping. The $D_x f$ is given as follows:

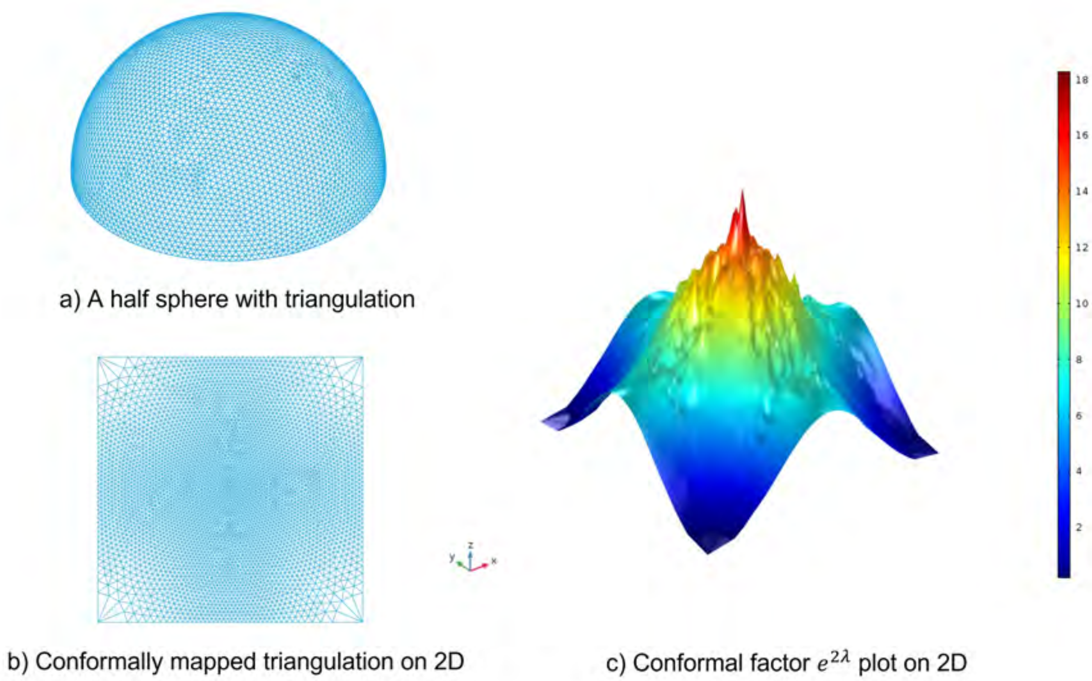

Figure 3: A conformal mapping of a half sphere to a 2D rectangle

$$
\begin{aligned}
D_x f &= lim_{\Delta x \to 0} \frac{f \circ \phi(x+\Delta x, y) - f \circ \phi(x,y)}{dist(x+\Delta x, x)} \\
&= lim_{\Delta x \to 0} \frac{f \circ \phi(x+\Delta x, y) - f \circ \phi(x,y)}{e^{\lambda} \Delta x} \\
&= e^{-\lambda} \frac{\partial f \circ \phi}{\partial x}
\end{aligned} \tag{3}
$$

$D_y f$ can be defined similarly. Then the gradient of f on the manifold can be represented as:

$$
\begin{aligned}
\nabla_M f &= \partial_x f \mathbf{i} + \partial_y f \mathbf{j} \\
&= e^{-\lambda} \frac{\partial f \circ \phi}{\partial x} \mathbf{i} + e^{-\lambda} \frac{\partial f \circ \phi}{\partial y} \mathbf{j},
\end{aligned} \tag{4}
$$

where $\mathbf{i} = e^{-\lambda} \frac{\partial}{\partial x}$, $\mathbf{j} = e^{-\lambda} \frac{\partial}{\partial y}$. For detailed derivations, interested readers are referred to [38, 42]. In this way, the Riemannian gradient can be expressed by the Euclidean differential operators multiplied by a scalar function. This provides a sound mathematical basis for the X-LSM and the DR-LSM proposed in this paper.

2.3. Extended level set method (X-LSM)

Resting on equation (4), in 2019 the authors [14] proposed the extended level set method (X-LSM) to address the shape and topology optimization problems on manifolds. The key idea of the

X-LSM is to transfer the conventional H-J equation from manifolds to the 2D parameter domain under conformal parameterization. Similar to the Euclidean H-J equation (2), the H-J equation on manifolds is given as follows:

$$\frac{\partial \Phi(\mathbf{x},t)}{\partial t} - V_n \cdot |\nabla_M \Phi| = 0, \tag{5}$$

where V_n is the normal velocity field on the manifold, $\nabla_M \Phi$ is the Riemannian gradient of Φ on the tangent plane of the manifold M. Let $\phi : \mathbb{R}^2 \to M$ be a conformal parameterization of M with a conformal factor $e^{2\lambda}$. We can then readily write the *modified H-J equation* on the Euclidean 2D parameter domain as below:

$$\frac{\partial \Phi(\mathbf{x},t)}{\partial t} - e^{-\lambda} V_n \cdot |\nabla \Phi| = 0. \tag{6}$$

In this way, the boundary evolution on the manifold embedded in the 3D space can be realized by solving the modified H-J equation on the 2D parameter domain. As such, the X-LSM elegantly extends the conventional level-set-based topology optimization methods from Euclidean space to general free-form surfaces, opening up a larger design space. In the authors' early work on X-LSM [14], only the H-J equation is transformed from manifolds to 2D parameter domain, but the finite element analysis (FEA) is still performed on the manifold.

2.4. Dimension reduction level set method (DR-LSM)

In this paper, we propose a dimension reduction level set method (DR-LSM) for shape and topology optimization on manifolds. In the DR-LSM formulation, both the H-J equation and the Laplace equation, which are the two PDEs governing boundary evolution and manifold heat conduction, are transformed from the manifold in 3D space to the 2D rectangular domain using conformal parameterization. In order to conduct the FEA also on the 2D parameter domain, we need to apply the conformal parameterization to the governing physics PDE to obtain a modified one defined on the 2D parameter domain. For the heat conduction problems studied in this paper, the governing equation is the Laplace equation, where there is no body heat source. One characteristic of the Laplace equation is its conformal invariance, meaning that the solutions are invariant under the conformal parameterization. A brief derivation for the plane to plane conformal mapping cases can be readily given as follows with the aid of complex analysis.

Consider the real-valued function $U(\xi,\eta)$ and the analytic map $w = f(z) = f(x+iy) = \xi(x,y) + i\eta(x,y)$, where ξ and η are real-valued functions. If $U(\xi,\eta)$ is a harmonic function of ξ and η, then the composition $u(x,y) = U(\xi(x,y),\eta(x,y))$ is also a harmonic function of x, y. To prove this, we first apply the chain rule below:

$$\frac{\partial u}{\partial x} = \frac{\partial U}{\partial \xi}\frac{\partial \xi}{\partial x} + \frac{\partial U}{\partial \eta}\frac{\partial \eta}{\partial x}, \frac{\partial u}{\partial y} = \frac{\partial U}{\partial \xi}\frac{\partial \xi}{\partial y} + \frac{\partial U}{\partial \eta}\frac{\partial \eta}{\partial y}. \tag{7}$$

$$\frac{\partial^2 u}{\partial x^2} = \frac{\partial^2 U}{\partial \xi^2}(\frac{\partial \xi}{\partial x})^2 + 2\frac{\partial^2 U}{\partial \xi \partial \eta}\frac{\partial \xi}{\partial x}\frac{\partial \eta}{\partial x} + \frac{\partial^2 U}{\partial \eta^2}(\frac{\partial \eta}{\partial x})^2 + \frac{\partial U}{\partial \xi}\frac{\partial^2 \xi}{\partial x^2} + \frac{\partial U}{\partial \eta}\frac{\partial^2 \eta}{\partial x^2}. \tag{8}$$

$$\frac{\partial^2 u}{\partial y^2} = \frac{\partial^2 U}{\partial \xi^2}(\frac{\partial \xi}{\partial y})^2 + 2\frac{\partial^2 U}{\partial \xi \partial \eta}\frac{\partial \xi}{\partial y}\frac{\partial \eta}{\partial y} + \frac{\partial^2 U}{\partial \eta^2}(\frac{\partial \eta}{\partial y})^2 + \frac{\partial U}{\partial \xi}\frac{\partial^2 \xi}{\partial y^2} + \frac{\partial U}{\partial \eta}\frac{\partial^2 \eta}{\partial y^2}. \tag{9}$$

Then the conformal mapping on 2D satisfies the Cauchy-Riemann equation:

$$\frac{\partial \xi}{\partial x} = -\frac{\partial \eta}{\partial y}, \frac{\partial \xi}{\partial y} = \frac{\partial \eta}{\partial x}. \tag{10}$$

After some algebra, we arrive at the following equation:

$$\Delta u = \frac{\partial^2 u}{\partial x^2} + \frac{\partial^2 u}{\partial y^2} = [(\frac{\partial \xi}{\partial x})^2 + (\frac{\partial \eta}{\partial x})^2](\frac{\partial^2 U}{\partial \xi^2} + \frac{\partial^2 U}{\partial \eta^2}) = |g'(z)|^2 \Delta U. \tag{11}$$

This equation implies that if u is harmonic in a region of the z-plane, U is also harmonic in a conformally mapped region of the w-plane.

When the heat equation is general with an arbitrary body heat source and boundary heat flux, it does not possess the conformal invariance property. In this case, we need to derive the modified heat equation under the conformal parameterization. Details are given in Section 4.

3. Conformal topology optimization of heat conduction problems on manifolds

3.1. Problem formulation

In this study, a stationary thermal conductivity problem is considered. All the material properties are assumed to be isotropic. The equations governing thermal conduction phenomena are as follows:

$$\begin{aligned} -k\nabla^2 T =&\ b,\ in\ \ \Omega \\ k\nabla T \cdot \mathbf{n} =&\ q,\ on\ \ \Gamma_N \\ k\nabla T \cdot \mathbf{n} =&\ 0,\ on\ \ \Gamma_H \\ T =&\ T_0,\ \ on\ \ \Gamma_D \end{aligned} \tag{12}$$

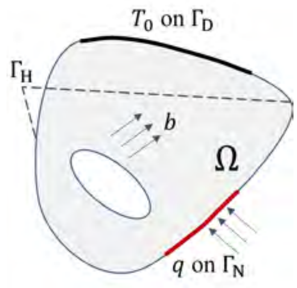

Figure 4: Diagram of a heat conductor

where k is the thermal conductivity; T is the state variable temperature; b is the rate of internal heat generation; $\mathbf{n}$ is the outward unit normal vector of the structural boundary; q is the heat flux in the inward normal direction. As shown in Figure 4, the structural boundaries are composed of a Dirichlet boundary Γ_D with $T = T_0$, a homogeneous Neumann boundary Γ_H which is adiabatic, and a non-homogeneous Neumann boundary Γ_N with a heat flux q. It is noted that when there is no body heat source, that is, $b = 0$, the heat equation is reduced to the Laplace equation, which holds the property of conformal invariance.

The weak form of the heat equations can be obtained by first multiplying a test function $\bar{T}$, integrating over the whole domain, utilizing the product rule, and applying the 2D divergence theorem with the boundary conditions as mentioned above. The weak form of the governing equation is as follows:

$$a(T,\bar{T}) = l(\bar{T}),\ \forall \bar{T} \in U_{ad} \tag{13}$$

where $\bar{T}$ is the test function for the temperature and U_{ad} is the space of the virtual temperature field meeting the same boundary condition. The bilinear function at the left side of equation (13) is defined as:

$$a(T,\bar{T}) = \int_{\Omega} k\nabla T \cdot \nabla \bar{T}\, d\Omega. \tag{14}$$

The linear function at the right side of equation (13) is defined as:

$$l(\bar{T}) = \int_{\Omega} b\bar{T}\, d\Omega + \int_{\Gamma_N} q\bar{T}\, ds. \tag{15}$$

The objective of the optimization problems is to minimize the thermal compliance under a volume constraint, which is set as follows:

$$
\begin{aligned}
&\underset{\Omega}{Inf} \quad J = \int_{\Omega} bT d\Omega + \int_{\Gamma_N} qT ds, \\
&S.t. \quad a(T,\bar{T}) = l(\bar{T}),\ \forall \bar{T} \in U_{ad} \\
&\qquad\quad V(\Omega) = V^*,
\end{aligned}
\tag{16}
$$

where $V(\Omega) = \int_{\Omega} dx$ denotes the volume of the design, and V^* is the target volume.

3.2. Shape sensitivity analysis

To evolve the structural boundaries by solving the Hamiltion-Jocabi equation under the level-set framework, the shape derivatives need to be conducted to provide a proper normal velocity field that can drive the boundary propagation toward the next better design [46, 47]. In this study, the material derivative method [82] and the adjoint method [83] are employed for the shape sensitivity analysis. The Lagrangian of the optimization problem is defined as

$$
L = J(T) + a(T,\bar{T}) - l(\bar{T}). \tag{17}
$$

The material derivative of the Lagrangian is given:

$$
\frac{DL}{Dt} = \frac{DJ(T)}{Dt} + \frac{Da(T,\bar{T})}{Dt} - \frac{Dl(\bar{T})}{Dt}. \tag{18}
$$

The material derivative of the objective function $J(T)$ is:

$$
\begin{aligned}
\frac{DJ(T)}{Dt} &= \int_{\Omega} (b'T + bT')d\Omega + \int_{\Gamma} bTV_n ds \\
&\quad + \int_{\Gamma} (q'T + qT')ds + \int_{\Gamma} (\frac{\partial (qT)}{\partial \mathbf{n}} + k_c qT) \cdot V_n ds.
\end{aligned}
\tag{19}
$$

The material derivative of the weak-form governing equation is:

$$
\begin{aligned}
&\frac{Da(T,\bar{T})}{Dt} - \frac{Dl(\bar{T})}{Dt} = \int_{\Omega} k[\nabla T' \cdot \nabla \bar{T} + \nabla T \cdot \nabla \bar{T}']d\Omega \\
&+ \int_{\Gamma} k\nabla T \cdot \nabla \bar{T} \cdot V_n ds - \int_{\Omega} (b'\bar{T} + b\bar{T}')d\Omega - \int_{\Gamma} b\bar{T} \cdot V_n ds \\
&- \int_{\Gamma} (q'\bar{T} + q\bar{T}')ds - \int_{\Gamma} (\frac{\partial (q\bar{T})}{\partial \mathbf{n}} + k_c q\bar{T}) \cdot V_n ds.
\end{aligned}
\tag{20}
$$

Collecting all the terms containing $\bar{T}'$ as follows:

$$\int_{\Omega} k\nabla T \cdot \nabla \bar{T}' d\Omega - \int_{\Omega} b\bar{T}' d\Omega - \int_{\Gamma} q\bar{T}' ds = 0. \tag{21}$$

The weak form of the state equation is retrieved as $a(T, \bar{T}') = l(\bar{T}')$, for $\forall \bar{T}' \in U_{ad}$. Assuming that the b and q are not time-dependent, and q is a nodal flux, the material derivatives for the Lagrangian can be rewritten as:

$$\begin{aligned} \frac{DL}{Dt} = & \int_{\Omega} bT' d\Omega + \int_{\Gamma} bTV_n ds + \int_{\Gamma} qT' ds \\ & + \int_{\Omega} k[\nabla T' \cdot \nabla \bar{T}] d\Omega + \int_{\Gamma} k\nabla T \cdot \nabla \bar{T} \cdot V_n ds \\ & - \int_{\Gamma} b\bar{T} \cdot V_n ds. \end{aligned} \tag{22}$$

By collecting the terms containing T' and making the sum equal to zero, one can obtain the adjoint equation:

$$\int_{\Omega} bT' d\Omega + \int_{\Gamma} qT' ds + \int_{\Omega} k[\nabla T' \cdot \nabla \bar{T}] d\Omega = 0. \tag{23}$$

We can readily solve the adjoint variable $\bar{T} = -T$. The remainder of the material derivatives of the Lagrangian is as follows:

$$\begin{aligned} \frac{DL}{Dt} = & \int_{\Gamma} bTV_n ds + \int_{\Gamma} k\nabla T \cdot \nabla \bar{T} \cdot V_n ds \\ & - \int_{\Gamma} b\bar{T} \cdot V_n ds. \end{aligned} \tag{24}$$

By substituting $\bar{T} = -T$ for the above equation and applying the steepest descent method, the design velocity field can be constructed as follows:

$$V_{n1} = -2bT + k\nabla T \cdot \nabla T. \tag{25}$$

For the volume constraint, the augmented Lagrangian method [82, 84, 85] is employed. The augmented objective function will be given as:

$$\hat{J} = J + \varphi(\Omega) = J + \lambda(V(\Omega) - V^*) + \frac{1}{2\mu}(V(\Omega) - V^*)^2, \tag{26}$$

where λ is the Lagrangian multiplier, and μ is a penalty parameter set by the designer and is close to zero. During the optimization process, the update schemes for λ and μ are as follows:

$$\begin{aligned} &\lambda^{k+1} = \max\{0, \lambda^k + \frac{1}{\mu^k}(V(\Omega) - V^*)\}, \\ &\mu^{k+1} = \alpha \cdot \mu^k, \end{aligned} \tag{27}$$

where $\alpha \in (0,1)$. After conducting the material derivative of $\varphi(\Omega)$ and applying the steepest descent method, the velocity field responsible for the volume constraint can be given as:

$$V_{n2} = -(\lambda + \frac{1}{\mu}(V(\Omega) - V^*)). \tag{28}$$

Another functional J_3 is introduced to for the boundary smoothing purpose, which is given as $J_3 = \alpha \int_\Gamma d\Gamma$ where α is a positive parameter. The velocity field accountable for J_3 is given as $V_{n3} = -\alpha k_c$, where k_c is the mean curvature.

Finally, the normal velocity field that drives the boundary evolution can be given as:

$$V_n = V_{n1} + V_{n2} + V_{n3} = -2bT + k\nabla T \cdot \nabla T - (\lambda + \frac{1}{\mu}(V(\Omega) - V^*)) - \alpha k_c. \tag{29}$$

4. Equivalent topology optimization of heat conduction problems on 2D parameter domain by DR-LSM

4.1. Modified heat equation on the 2D parameter domain

Figure 5 illustrates the workflow for the proposed method. The first step is to conformally map the manifold in 3D space to a 2D rectangular parameter domain, where the level-set function is initialized to give the initial design. In the proposed DR-LSM, consistency between the geometrical and physics models is maintained. That is, we apply the conformal parameterization not only to the geometrical model but also to the physics equation. On the 2D parameter domain, we need to conduct the FEA with a modified heat equation. Applying the same principle as in Section 2.2.2, the modified heat equation under the conformal parameterization is given in equation (30) as follows:

$$\begin{aligned} &-k \cdot e^{-2\lambda} \nabla^2 T = \ b, \ in \ \ S \\ &k \cdot e^{-\lambda} \nabla T \cdot \mathbf{n}_1 = q, \ on \ \ \Gamma_{N1} \\ &k \cdot e^{-\lambda} \nabla T \cdot \mathbf{n}_1 = 0, \ on \ \ \Gamma_{H1} \\ &T = T_0, \ \ on \ \ \Gamma_{D1} \end{aligned} \tag{30}$$

where $e^{2\lambda}$ is the conformal factor associated with this conformal parameterization and $\mathbf{n}_1$ is the outward unit normal vector on the 2D parameter domain.

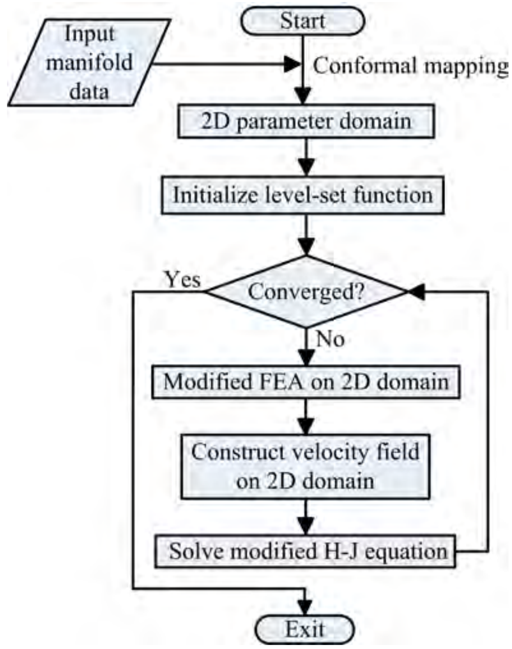

Figure 5: The flowchart of the DR-LSM

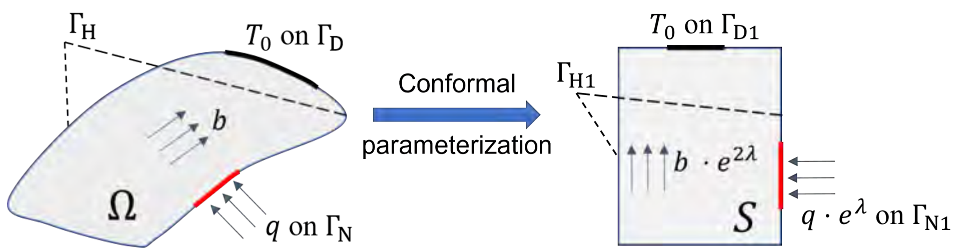

Figure 6: The boundary condition correspondences

The correspondences of boundary conditions is also illustrated in Figure 6. The whole structural boundary of the original manifold Ω consists of a Dirichlet boundary Γ_D with $T = T_0$, a homogeneous Neumann boundary Γ_H and a non-homogeneous Neumann boundary Γ_N. There is also a uniform body heat source b over the original design domain Ω. As part of the conformal parameterization, we need to make proper modifications to the boundary conditions on the 2D parameter domain. For the body heat source, we assign an equivalent value of $b \cdot e^{2\lambda}$ on the 2D parameter domain, where $e^{2\lambda}$ is the conformal factor associated with this conformal parameterization. Geometrically, the conformal factor stands for the area ratio between the original manifold and 2D parameter domain, which varies from point to point. Physically, this modification of the body heat source makes sense in that the integral of the body heat source over the domain gives the total power imported into the system. Therefore, such a modification on the body heat source can keep the same total energy input for the manifold and the 2D parameter domain.

As for the Dirichlet boundary, we assign the same T_0 to the correspondingly mapped boundary Γ_{D1} on the 2D parameter domain since the scalar field T does not change its value under the conformal mapping. As far as the Neumann boundary conditions are concerned, an equivalent heat flux $q \cdot e^{\lambda}$ is assigned on the correspondingly mapped non-homogeneous Neumann boundary

Γ_{N1} on the 2D parameter domain. Physically, this makes sense in that the integral of the heat flux along the non-homogeneous Neumann boundary actually gives the power, which can be seen as the energy source into the system. Due to the scaling effect of the conformal parameterization, the length of the non-homogeneous Neumann boundary on the manifold differs a factor of e^{λ} from that on the 2D parameter domain. Assuming the manifold and the 2D parameter domain share the same thickness, then the heat flux on the 2D domain can be approximately given as $q \cdot r$, where r is the ratio between the length of the non-homogeneous Neumann boundary on the manifold and the 2D parameter domain. The remaining boundary Γ_{H1} corresponding to the adiabatic Γ_H on the original manifold will still be adiabatic.

4.2. Modified problem-setting on the 2D parameter domain

In a typical implementation of the level-set-based topology optimization, the objective function, the current volume, and the velocity field are usually evaluated where the FEA is conducted. In this study, since the FEA is transferred onto the 2D parameter domain, we want to compute the above three quantities equivalently on the 2D domain. On the original manifold, the expressions for the objective function, the current volume, and the normal speed are respectively given as follows:

$$
\begin{aligned}
J &= \int_{\Omega} k \nabla_M T \cdot \nabla_M T \, d\Omega, \\
V &= \int_{\Omega} d\Omega, \\
V_{nT} &= -2bT + k \nabla_M T \cdot \nabla_M T,
\end{aligned}
\tag{31}
$$

where V_{nT} is the normal velocity component directly pertaining to the Lagrangian L (see equation (29)). Under the conformal parameterization, the above formulas should be properly modified as below according to Section 2.2.2:

$$
\begin{aligned}
J &= \int_{S} k \nabla T \cdot \nabla T \, dS, \\
V &= \int_{S} e^{2\lambda} dS, \\
V_{nT} &= -2bT + k \cdot e^{-2\lambda} \nabla T \cdot \nabla T.
\end{aligned}
\tag{32}
$$

In this way, the objective function, current volume, and the normal velocity field can now be equivalently evaluated on the 2D parameter domain.

4.3. Equivalence of the DR-LSM formulation

This sub-section summarizes the key ingredients of the DR-LSM formulation and emphasizes the equivalence of this dimension reduction. The fact that the optimality of the target problems is maintained after conformal mapping will be briefly justified.

The original topology optimization problem defined on a general free-form surface in 3D space is essentially a PDE-constrained optimization problem. It involves solving the governing physics equation to obtain the state variables, based on which the objective function J, current volume V, and normal velocity V_n are evaluated in the level set framework. In the DR-LSM formulation proposed in this paper, the governing equation is solved equivalently on the 2D rectangle domain using conformal parameterization. Geometrically, a one-to-one mapping relation from the manifold to the 2D rectangle domain is found by the conformal mapping algorithm as shown in Figure 3. Note that the conformal mapping algorithm works with triangulation.

With the conformal parameterization, the differential operators defined on the manifolds can be transferred into their Euclidean forms with a combination of the conformal factor $e^{2\lambda}$ describing the scaling effect of the conformal mapping. The derivation process is detailed in subsection 2.2. Resting on equation (4), we can readily derive the modified PDE to be solved on the 2D parameter domain. Taking the pure heat conduction problem studied in this paper as an example, the modified heat equation is given in Figure 7. Recall that the conformal mapping gives a one-to-one mapping between a triangulation vertex on the original manifold and the 2D parameter domain (see Figure 3). Suppose a vertex A on the manifold is mapped to vertex A' on the 2D parameter domain. Since the state variable for the pure heat conduction problem is a scalar temperature field T, it does not change its value under conformal mapping. By solving the modified heat equation on the 2D parameter domain, the temperature T'_A at vertex A' will be the same as T_A at original vertex A, which could be obtained by solving the original heat equation directly on the manifold. This relation will hold for all the A-to-A' pairs, i.e., there also exists a mapping between the temperature fields T and T', obtained by solving the original heat equation on the manifold and the modified heat equation on 2D parameter domain, respectively.

As for the related physical quantities, i.e., objective function, current volume, and normal velocity, they all have an appropriately modified form according to the conformal parameterization as shown in Figure 7. This modification makes sure that no matter where you conduct the finite element analysis, on the manifold or the 2D rectangle domain, the above three physics quantities will have the same evaluated values for a specific material distribution during the optimization process. Thus, the equivalence of performing the finite element analysis on the 2D parameter domain by solving a modified heat equation is justified.

Another involved PDE is the Hamilton-Jacobi equation, which is solved iteratively to update the level set function to drive the evolution of the structural boundary. As a major contribution of the paper [14] from our research group, the *modified Hamilton-Jacobi equation* given as equation (6) is obtained by applying the conformal parameterization on the original Hamilton-Jacobi equation defined on the manifold. The modified H-J equation is equivalently solved on the 2D parameter domain to circumvent the hurdle of structural boundary evolution directly on the original manifold. In the DR-LSM formulation, we still resort to the modified H-J equation (also shown in Figure 7) to update the level set function and evolve the structural boundary on the 2D parameter domain.

To sum up, the optimality of the target optimization problem is maintained after the conformal mapping in the DR-LSM formulation. It is not only justified by the above mathematical derivation and reasoning but also demonstrated using the first three numerical examples in Section 6.1, 6.2 and 6.3. Specifically, the comparisons between the results obtained by the conventional X-LSM and the proposed DR-LSM are quite promising and convincing. The optimal designs obtained from X-LSM and DR-LSM are almost identical for those above three numerical examples. There is little discrepancy in the final objective function value. The volume constraints are satisfied for both methods. All these support the point that the optimality of the original optimization problems is maintained in the DR-LSM formulation.

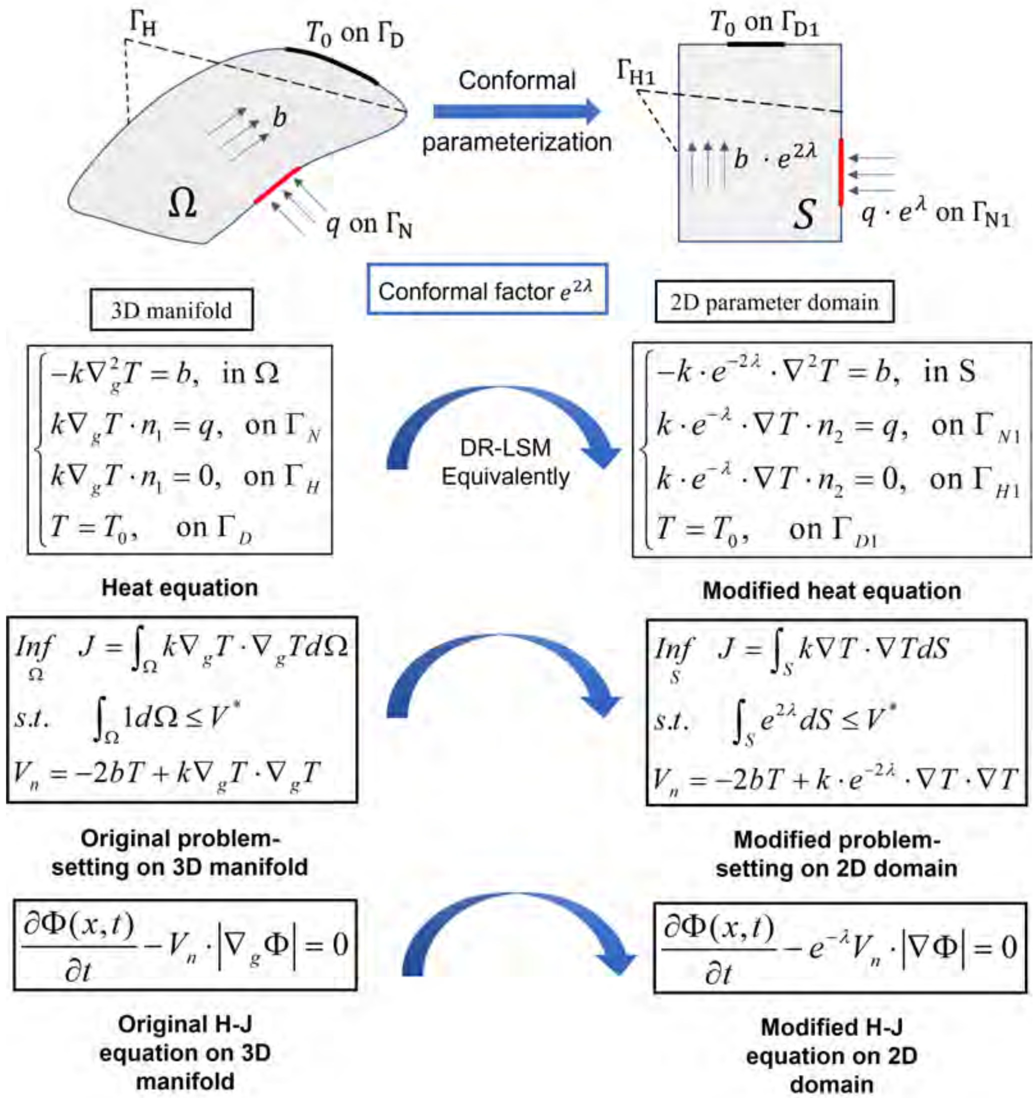

Figure 7: The summary of DR-LSM formulation

5. Numerical implementation

5.1. Algorithm

Here, we present the algorithm in Alg. 1 to implement the proposed DR-LSM. First, a triangulated manifold model Ω in 3D space is imported to define the original topology optimization problem. Then, we apply the conformal parameterization both geometrically and physically. Geometrically, the manifold Ω is conformally mapped to a 2D rectangle, which will serve as the 2D parameter domain S. Physically, we apply the conformal parameterization to the governing equation to obtain a modified heat equation on S. Besides, the related physics quantities, e.g., the objective function, current volume, and normal velocity, will have a properly modified form on S.

Then, the level set function Φ is initialized on S, and the modified heat equation is solved to obtain the temperature field T, from which the design velocity field is constructed. Finally, the level set function is updated by solving the modified H-J equation on S to evolve the structural boundaries. Steps 5-7 are repeated until the convergence criterion is satisfied. In this paper, the convergence criterion of the optimization is $|J_i - J_{i+1}|/J_i \leq \varepsilon$, where ε is a small parameter.

Algorithm 1: A DR-LSM for Shape and Topology Optimization on Manifolds

Input: A triangulated manifold Ω with original problem-setting defined on it
Output: The 3D minimum thermal compliance design
1 Conformally map the manifold Ω to a 2D rectangle parameter domain S;
2 Apply the conformal parameterization to the governing equations to obtain a modified heat equation;
3 Modify the expressions for related physics quantities properly to be evaluated on S;
4 Initialize the level set function Φ on S;
5 Solve the modified heat equation on S;
6 Construct the design velocity field on S;
7 Update the level set function Φ by solving the modified H-J equation on S until convergence;
8 Obtain the final optimized design on Ω from Φ;

6. Numerical examples

In this section, several numerical examples are provided to demonstrate the effectiveness of the proposed methodology. Some comparisons between the proposed DR-LSM and the conventional X-LSM are also given to exhibit the computational savings due to the dimension reduction formulation. These numerical examples differ in both geometrical model complexity and physical boundary conditions. The dimensions are given in meters for all the numerical examples with an even thickness of 0.01.

6.1. Spherical surface patch with boundary heat flux

The first numerical example is a spherical surface patch as the manifold shown in Figure 8 with the boundary conditions. The surface model can be obtained by partitioning a semi-spherical surface with two parallel planes. A Dirichlet boundary condition of $T = 0$ is assigned to the top and bottom curve segments in blue color. A heat flux of $q = 10W/m^2$ is applied to the two laterial curve segments represented in red. The adiabatic thermal boundary condition is applied to other edges. Mathematically, the governing equation corresponds to the Laplace's equation, which possesses the property of conformal invariance. These four curve segments in color sit in the middle with the length set at $1/10$ of the respective boundary edge lengths. The overall size of the manifold is $1{\times}1.4{\times}2$. The volume ratio target is set as $V_f = 0.4$. The thermal conductivity of the solid material is given as $k = 10W/(m*K)$. To avoid singularity, an ersatz material model is employed with $k = 0.001W/(m*K)$ for the weak material.

The initial and optimized designs on the 2D parameter domain and the original manifold obtained using the proposed DR-LSM and X-LSM are shown in Figure 9. The 2D parameter domain

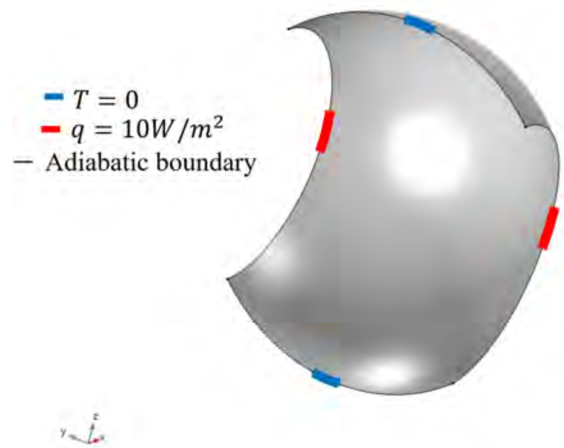

Figure 8: Boundary conditions of the spherical surface patch with boundary heat flux

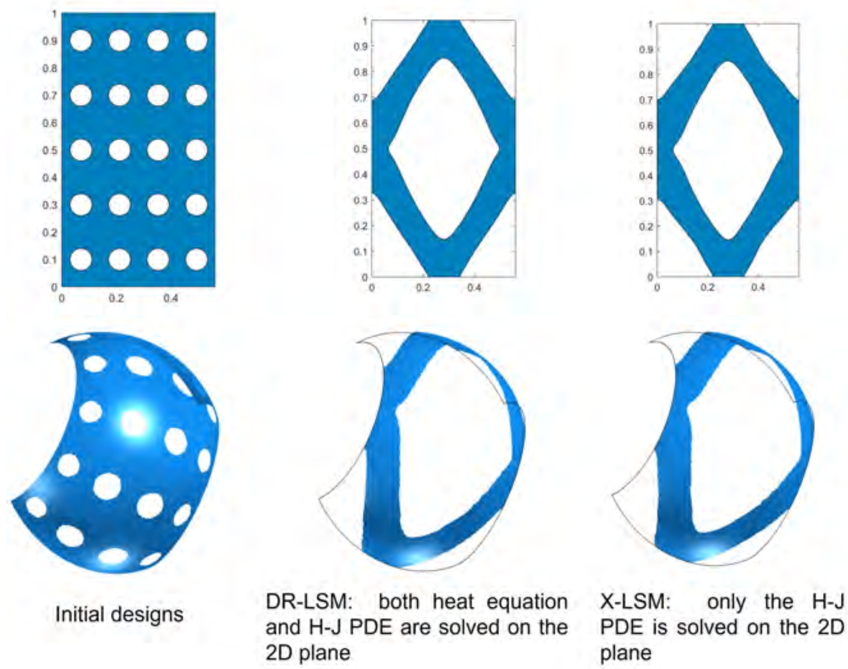

Figure 9: Initial and optimized designs for the spherical surface patch with boundary heat flux

is a 0.5625×1 rectangle. According to subsection 4.1, the heat flux on the non-homogeneous Neumann boundary of the 2D parameter domain is set to be $q \cdot r = 10 \times 2.093 = 20.93\ W/m^2$. There is little difference between the final optimized results achieved using the proposed DR-LSM and the conventional X-LSM with FEA performed on the manifold. In addition, the results are consistent with a 2D version heat conduction topology optimization result with similar boundary conditions [76]. The convergence history plots are given in Figure 10. The $V_f = 0.4$ volumetric constraint is met for both methods. It is worth noting that the objective function values are respectively 3.2058 and 3.2842 for our proposed DR-LSM and the conventional X-LSM. The discrepancy of the thermal compliance is only 2.39% and is well within the acceptable range, demonstrating

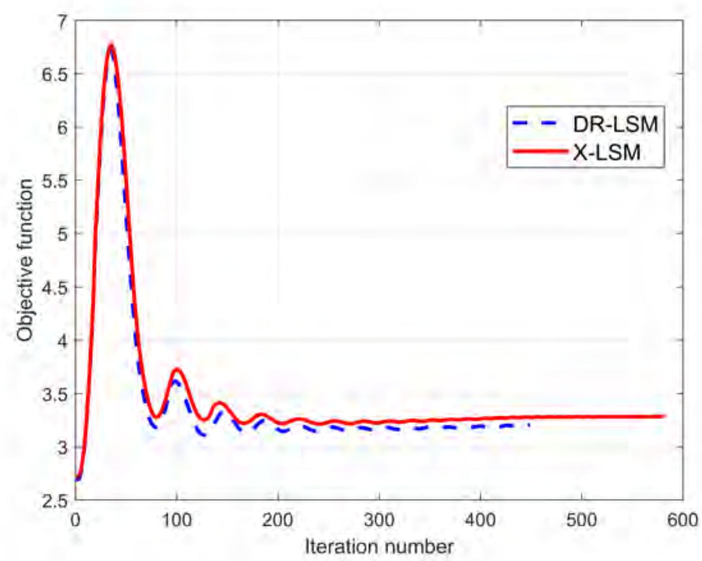

Figure 10: Convergence history of the spherical surface patch with boundary heat flux

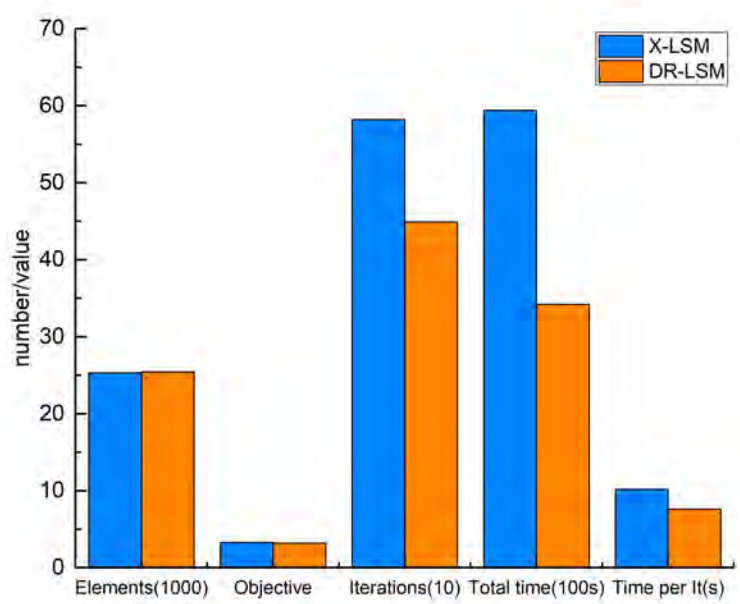

Figure 11: Comparisons between DR-LSM and X-LSM for example 6.1

the equivalence of conducting FEA on the 2D parameter domain.

In order to illustrate the advantage of the proposed DR-LSM in saving the computational cost, a comparison is given in Table 1. As shown in Table 1, the DR-LSM uses a total of 25442 triangular elements, slightly higher than the X-LSM's 25310. The DR-LSM runs only 449 total iterations before convergence while the X-LSM performs 582 iterations to attain optimized design. In terms of the total computation time and time per iteration, the DR-LSM costs 3420s and 7.62s compared to the X-LSM's 5940s and 10.2s, respectively. Specifically, the reduction by DR-LSM in terms of total time and time per iteration can be up to 42% and 25.3%, respectively, which is rather

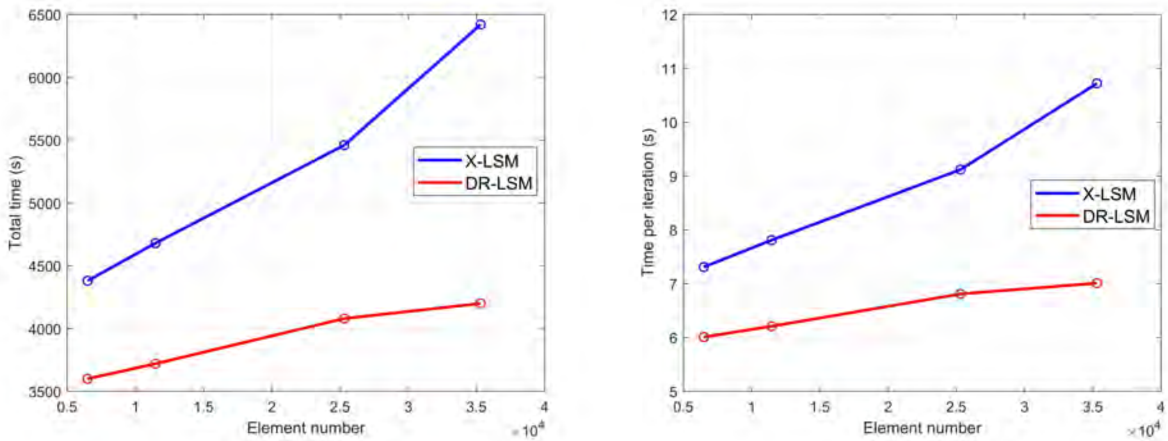

Figure 12: The computational time versus finite element number for example 6.1. Left: total time. Right: average time per iteration

promising. The reason for the decrease in computational costs will be further explained in Section 7. A bar graph is presented in Figure 11 to clearly show the differences between DR-LSM and X-LSM.

Table 1: Computational cost comparisons for example 6.1

Method	Mesh type	Element number	Obj	Total iterations	Total time	Time per It
X-LSM	Triangular	25310	3.2842	582	5940s	10.2s
DR-LSM	Triangular	25442	3.2058	449	3420s	7.62s

Reduction by DR-LSM	
Total time	Avg. time
42%	**25.3%**

The scalability of the computational cost-saving capacity brought by the proposed DR-LSM against the X-LSM is illustrated by plotting the computational time to the element number. For the sake of conciseness of this paper, this comparison is made using only the first numerical example, i.e., spherical surface patch with boundary heat flux. As shown in Figure 12, the total computational time and average time per iteration are plotted against the number of finite elements for both the X-LSM and the proposed DR-LSM. The computational time monotonically increases as a larger number of finite elements mean a lot more DOFs and longer solving time. The DR-LSM costs less computational time for various mesh fineness compared with the X-LSM. Another interesting observation we can make is that the finer the mesh is, the more relative computational cost savings we will get from the DR-LSM. Specifically, for the four data points in Figure 12, the triangular elements numbers are 6500, 11472, 25310, 35300, respectively. For the total computational time and average time per iteration, the DR-LSM can save 17.78%, 20.49%, 25.33%, and 34.61%, respectively, compared with the X-LSM.

6.2. Spherical surface patch with body heat source

The second numerical example is also a spherical surface patch but with a uniform body heat source, as illustrated in Figure 13. A Dirichlet boundary condition $T = 0$ is assigned to the bottom curve segment in blue color. A uniform heat source $b = 10W/m^3$ is applied all over the design domain. The adiabatic thermal boundary condition is applied to other edges. Mathematically, the governing equation is the Poisson's equation. The curve segment in blue color sits in the middle with the length set at $1/5$ of the length of the bottom edge. The size of the manifold is $1\times1.4\times2$. The volume ratio target is set as $V_f = 0.4$. The thermal conductivity of the solid material is given as $k = 10W/(m*K)$. To prevent singularity in finite element analysis, an ersatz material model is employed with $k = 0.1W/(m*K)$ for the weak material.

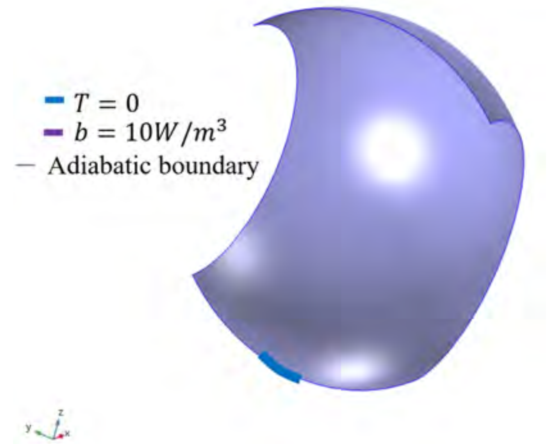

Figure 13: Boundary conditions of the spherical surface patch with body heat source

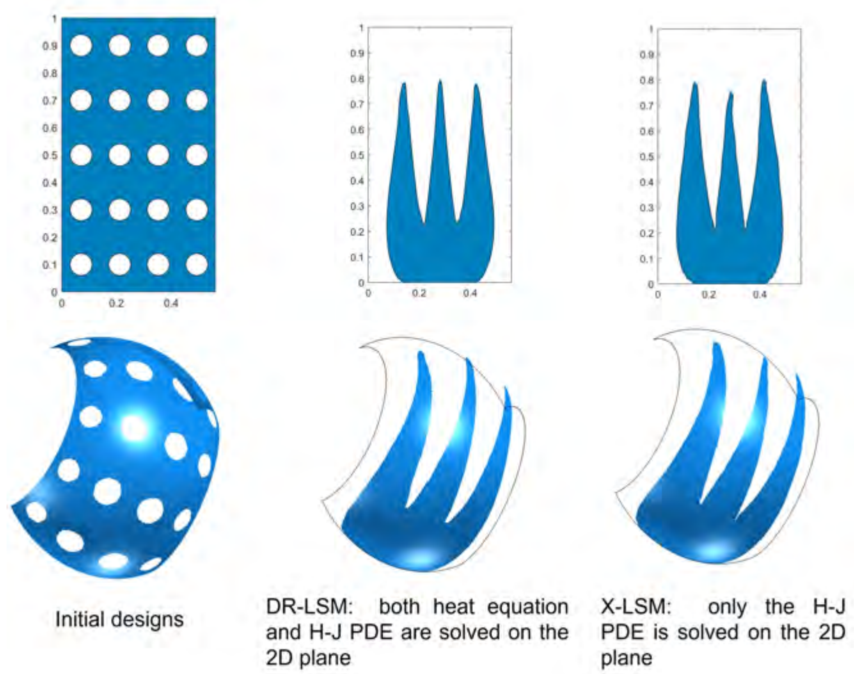

Figure 14: Initial and optimized designs for the spherical surface patch with body heat source

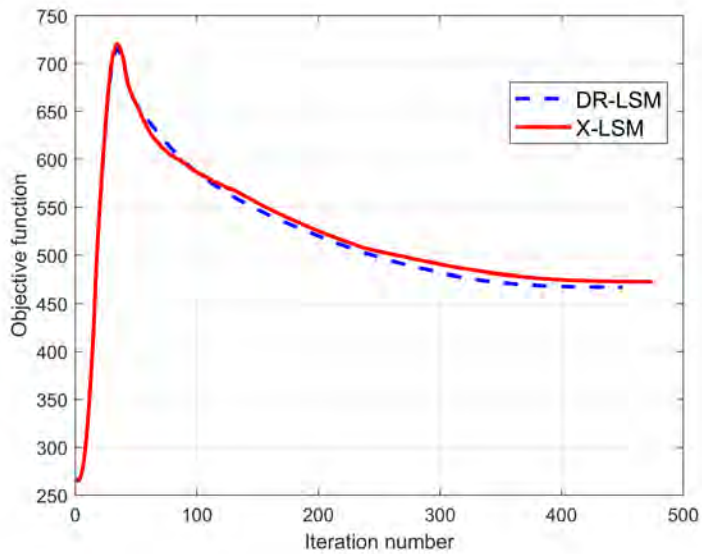

Figure 15: Convergence history of the spherical surface patch with body heat source

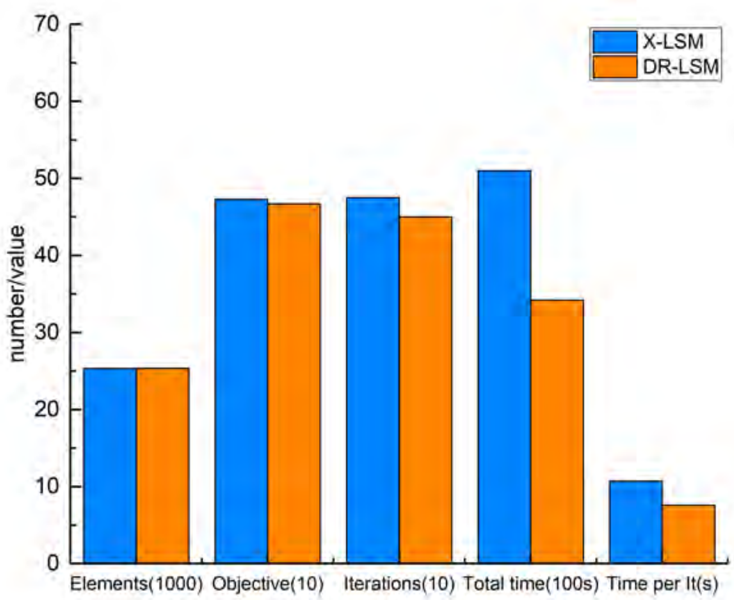

Figure 16: Comparisons between DR-LSM and X-LSM for example 6.2

The initial and optimized designs on the 2D parameter domain and the original manifold obtained using the proposed DR-LSM and X-LSM are shown in Figure 14. The 2D parameter domain is a 0.5625×1 rectangle. According to the subsection 4.1, the body heat source on the 2D parameter domain is modified to be $b \cdot e^{2\lambda} = 10\ e^{2\lambda}\ W/m^2$, where $e^{2\lambda}$ is the conformal factor associated with this conformal parameterization and it will vary from point to point. The designs obtained from the proposed DR-LSM and the conventional X-LSM where the FEA is still conducted on the manifold show little difference. In other words, both methods are consistent with one the other, demonstrating the feasibility of the proposed DR-LSM. The convergence history plots are provided in Figure 15. The volume ratio target $V_f = 0.4$ is achieved for both methods. It is promising that the thermal compliance values are 467.1 and 472.9, respectively, for our proposed DR-LSM and the conventional X-LSM. The discrepancy of the objective function is only 1.23% and can be neglected.

Table 2 is given with a detailed comparison on the computational cost taken by the proposed DR-LSM and the conventional X-LSM to fully display the advantage of the former. Specifically, in Table 2, it is shown that the X-LSM utilizes in total 25344 triangular elements, slightly less than DR-LSM's 25356. The numbers of total iterations before convergence are 450 and 475, respectively, for the proposed DR-LSM and the X-LSM. As far as the total computational time and time per iteration are concerned, the DR-LSM's 3420s and 7.6s, respectively, outweigh the X-LSM's 5100s and 10.7s, respectively. To be more accurate, the DR-LSM reduces 32.9% of the total time and 29.2% of the average time per iteration compared with the X-LSM. Figure 16 depicts the comparisons between DR-LSM and X-LSM in a more intuitive way.

Table 2: Computational cost comparisons for example 6.2

Method	Mesh type	Element number	Obj	Total iterations	Total time	Time per It
X-LSM	Triangular	25344	472.9	475	5100s	10.7s
DR-LSM	Triangular	25356	467.1	450	3420s	7.6s

Reduction by DR-LSM	
Total time	Avg. time
32.9%	**29.2%**

6.3. *Quarter Schwarz P TPMS surface with nodal heat source*

The third numerical example is a quarter Schwarz P triply periodic minimal surface (TPMS) with a central nodal heat source. One interesting geometrical feature of a TPMS is its large surface area, which is suitable for applications like chemical reactions or heat and mass transfer [86]. A TPMS can be approximated by a level-set equation. Taking the Schwarz P surface as an example, the approximation can be given as:

$$\phi_P \equiv cos\ x + cos\ y + cos\ z = c, \tag{33}$$

where c is a constant. A Schwarz P surface is shown in Figure 17. We select a quarter of Schwarz P TPMS to serve as the design domain. The boundary conditions are shown in Figure 18. A Dirichlet boundary condition $T = 0$ is assigned to the six boundary segments in blue. The top and bottom four boundary segments in blue are symmetric, and each accounts for $1/8$ of the respective boundary edge lengths. The remaining two boundary segments in blue sit in the middle with the length set as $1/16$ of the respective boundary edge lengths. Two nodal heat sources $q = 10W$ are applied in the center of the top and bottom half of the model represented in red. All other boundaries are adiabatic. The overall size of the Schwarz P TPMS unit is 6.2×6.2×6.2. For the quarter unit cell, the overall size is 3.1×3.1×6.2. The volume ratio target is set to $V_f = 0.4$. The thermal conductivity for the solid material is given as $k = 10W/(m*K)$. To avoid singularity, an ersatz material model is employed with $k = 0.001W/(m*K)$ for the weak material.

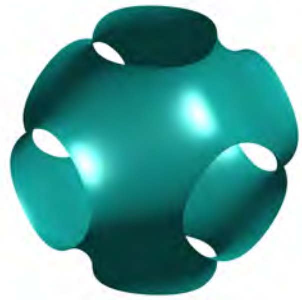

Figure 17: A Schwarz P surface

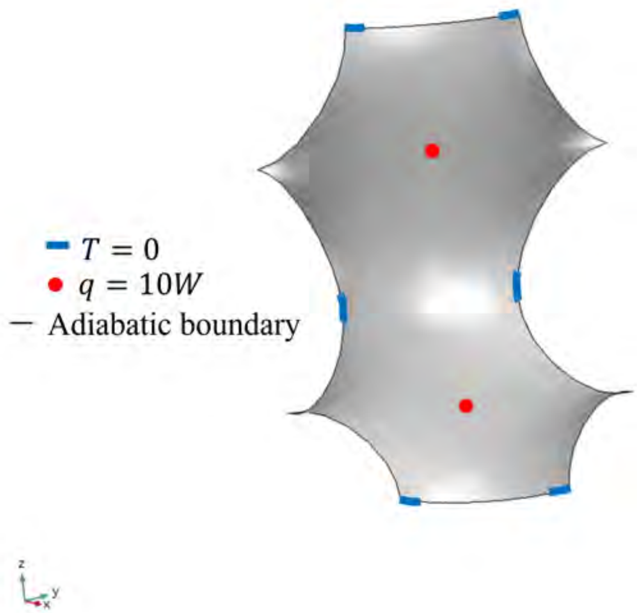

Figure 18: Boundary conditions of the quarter Schwarz P surface

The initial and optimized designs on the 2D parameter domain and the original manifold obtained using the proposed DR-LSM and X-LSM are shown in Figure 19. The 2D parameter domain is a 0.3958×1 rectangle. Based on subsection 4.1, the nodal heat source is still $q = 10W$ on the 2D parameter domain. Physically, it makes sense in that the total energy input is kept the same for the original manifold and the 2D parameter domain. The results obtained by the proposed DR-LSM and by the conventional X-LSM are almost identical. Figure 20 shows the convergence history plots. The volume constraint $V_f = 0.4$ is satisfied for both methods. The final objective function values are 34.34 and 33.64 for the DR-LSM and the conventional X-LSM, respectively. The discrepancy of the objective function values is only 2.04% and is in the negligible range, which shows the validity of the proposed DR-LSM. The final optimized design on the Schwarz P TPMS unit is shown in Figure 21 with different views.

It can be observed that there are some fluctuations in the convergence history plots in Figure 10 and 20. A brief explanation is provided here. In this paper, we enforce the volume constraint using the augmented Lagrangian method, which seeks to find the optimum of the original con-

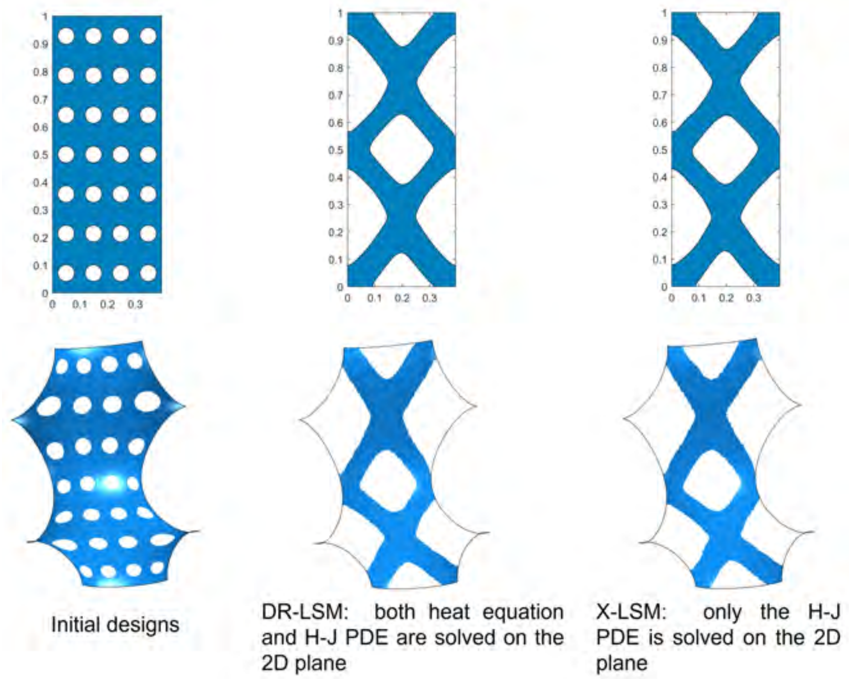

Figure 19: Initial and optimized designs for the quarter Schwarz P with nodal heat source

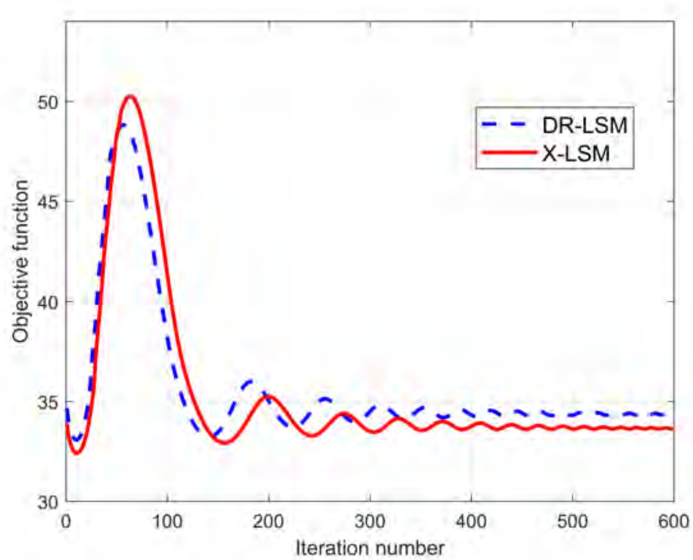

Figure 20: Convergence history of the quarter Schwarz P with nodal heat source

strained optimization problem by solving a series of unconstrained problems. According to the shape sensitivity analysis in subsection 3.2, the final normal velocity V_n mainly consists of two components V_{n1} and V_{n2} as shown in equation (29). Analogous to the minimum compliance optimization problem in linear elasticity, the problem-setting tends to fill the whole reference domain with solid material to reduce the thermal compliance when there is no volume constraint imposed. For the initial designs, a greater amount of solid material than the volume target is given in order to

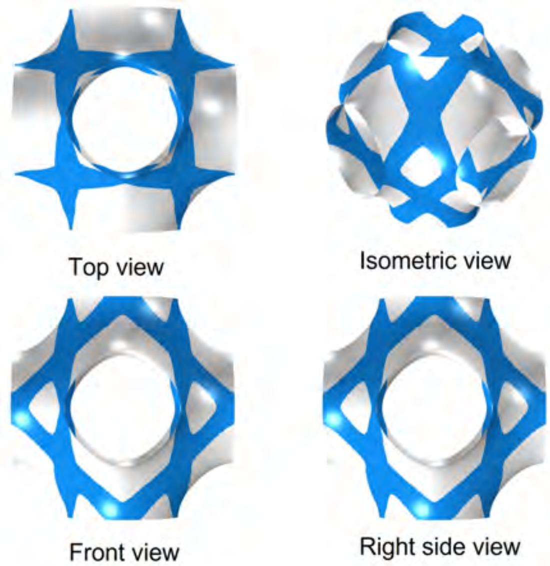

Figure 21: Final design on a Schwarz P TPMS unit

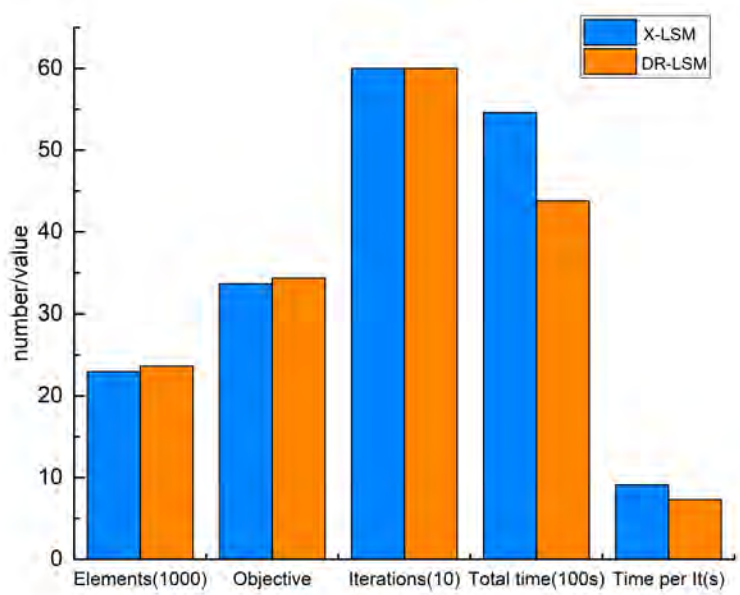

Figure 22: Comparisons between DR-LSM and X-LSM for example 6.3

let the volume constraint play a role in the evolution of structures. In the early optimization stage, the above normal velocity component V_{n2} derived from the volume constraint will be dominant to remove excess solid material. When the remaining solid material fraction is below the volume target, the effect of V_{n2} will gradually decline. Then the normal velocity component V_{n1} derived from the objective function J will take primary effect to add some solid material back. The "battle" between V_{n1} and V_{n2} could span a number of iterations, where the change of dominance is reflected as the fluctuations in the convergence history plots. This fluctuation is not uncommon when the volume constraint is enforced using the augmented Lagrangian method. A similar convergence history plot can be found in [84]. One advantage of the augmented Lagrangian method is that it can ensure accurate enforcement of the volume constraint.

Table 3 details the comparisons between the proposed DR-LSM and the conventional X-LSM as far as the computational costs are concerned. Both the DR-LSM and the X-LSM employ the triangular mesh type with a very close number of elements (23616 and 22958, respectively). Both methods iterate 600 times. In terms of total computational time and average time per iteration, the DR-LSM consumes 4380s and 7.3s, respectively, compared with X-LSM's 5460s and 9.1s, respectively. The DR-LSM can save 19.78% in total computational time and average time per iteration as opposed to the X-LSM. Figure 22 shows a clearer view of the comparisons between DR-LSM and X-LSM.

Table 3: Computational cost comparisons for example 6.3

Method	Mesh type	Element number	Obj	Total iterations	Total time	Time per It
X-LSM	Triangular	22958	33.64	600	5460s	9.1s
DR-LSM	Triangular	23616	34.34	600	4380s	7.3s

Reduction by DR-LSM	
Total time	Avg. time
19.78%	**19.78%**

6.4. *Vase with body heat source*

Through the first three numerical examples(Section 6.1, 6.2 and 6.3), the validity and advantages of the proposed DR-LSM are illustrated by the comparisons with the conventional X-LSM. The fourth numerical example is a vase with a uniform body heat source, which is solely tackled by the DR-LSM to make this paper concise. The vase has a through hole and the boundary conditions are shown in Figure 23. A Dirichlet boundary condition $T = 0$ is assigned to the bottom circular boundary edge in blue color. A uniform heat source $b = 1W/m^3$ is applied all over the design domain. The adiabatic thermal boundary condition is applied to other edges. The overall size of this manifold is 3.4×3.4×3.7. The volume ratio target is set to be $V_f = 0.4$. The thermal conductivity for the solid material is given as $k = 10W/(m*K)$. To avoid singularity, an ersatz material model is employed with $k = 0.1W/(m*K)$ for the dummy material.

The design evolution on the 2D parameter domain and the original vase manifold are shown in Figure 24. The 2D parameter domain is a 1.5126×1 rectangle, where the modified heat equation is solved with a triangular mesh of 67014 elements. Similar to the spherical surface patch example with body heat source in Section 6.2, an equivalent body heat source $b \cdot e^{2\lambda} = e^{2\lambda}\ W/m^2$ is assigned on the 2D parameter domain, where $e^{2\lambda}$ is the conformal factor associated with this conformal parameterization and it will vary from point to point. The convergence history plot is shown in Figure 25. The final objective function value is 80.92, and the volume ratio target of 0.4 is satisfied.

6.5. *Human face with nodal heat sources*

The fifth numerical example is a scanned human face with multiple nodal heat sources as shown in Figure 26. For the sake of brevity, this example is also only solved by the proposed DR-LSM. This surface model has no geometrical symmetry. There are a total of 7 nodal heat sources with $q = 1W$. A Dirichlet boundary condition $T = 0$ is assigned to the boundary segment in blue. All remaining boundaries are kept adiabatic. The overall size of this manifold is

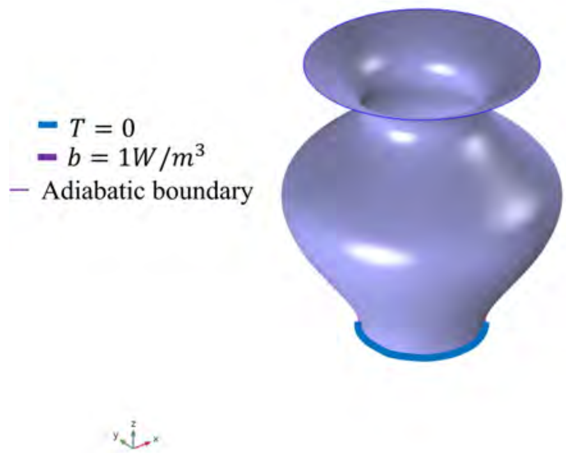

Figure 23: Boundary conditions of the vase surface with body heat source

$1.0875\times0.9254\times1.5778$. The target for the volume ratio is 0.4. The thermal conductivity of the solid material is given as $k = 10W/(m*K)$. To avoid singularity, an ersatz material model is employed with $k = 0.001W/(m*K)$ for the dummy material.

The design evolution on the 2D parameter domain and the original human face manifold are shown in Figure 27. The 2D parameter domain is a 0.8849×1 rectangle, where the modified heat equation is solved with a triangular mesh of 42297 elements. Similar to the quarter Schwarz P TPMS surface example with nodal heat sources in Section 6.3 in terms of boundary condition correspondences, there will be 7 nodal heat sources with $q = 1W$ on the 2D parameter domain. The convergence history plot is given in Figure 28. The final objective function value is 9.57, and the volume ratio constraint of 0.4 is satisfied. Here, we give some explanations on the final optimized design on the human face. First, the final design does not exhibit symmetry because neither the human face pattern nor the nodal heat sources are symmetrical. Second, the objective function of this optimization problem is thermal compliance. Minimizing the thermal compliance is equivalent to minimizing the mean temperature of the domain. When there is no body heat source, the final optimized design tends to connect the nodal heat source or boundary heat flux with the Dirichlet boundary $T = 0$ with a shorter path so that the heat generated from the source or flux can be quickly conducted over the domain to reduce the mean temperature. This tendency may also be observed from the first and third numerical examples in Section 6.1 and Section 6.3, respectively. Then the final optimized design shown in the last column in Figure 27 makes sense in that the 7 nodal heat sources are connected to the bottom Dirichlet boundary with relatively short paths. It is most obvious for the nodal heat source located in the central forehead region as its pathway to the Dirichlet boundary circumvents the nose tip to avoid a longer conduction path.

7. Discussions and conclusions

7.1. The computational cost saving by DR-LSM

In this paper, we propose a new dimension reduction level set method (DR-LSM) for shape and topology optimization by incorporating the conformal geometry theory. As part of the conformal parameterization, the original topology optimization problem defined on a general free-form

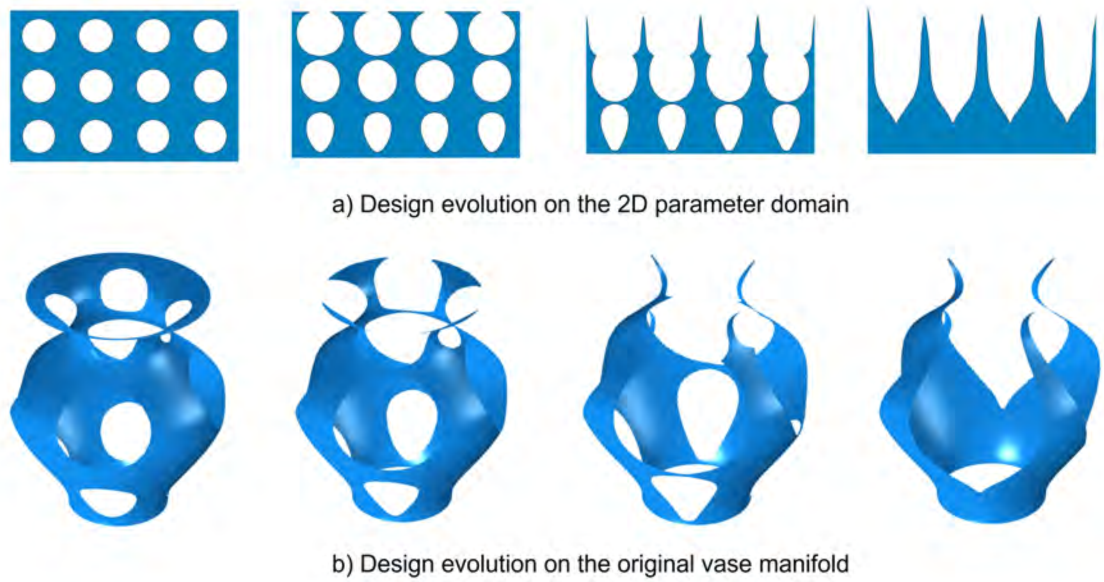

Figure 24: The design evolution of the vase example

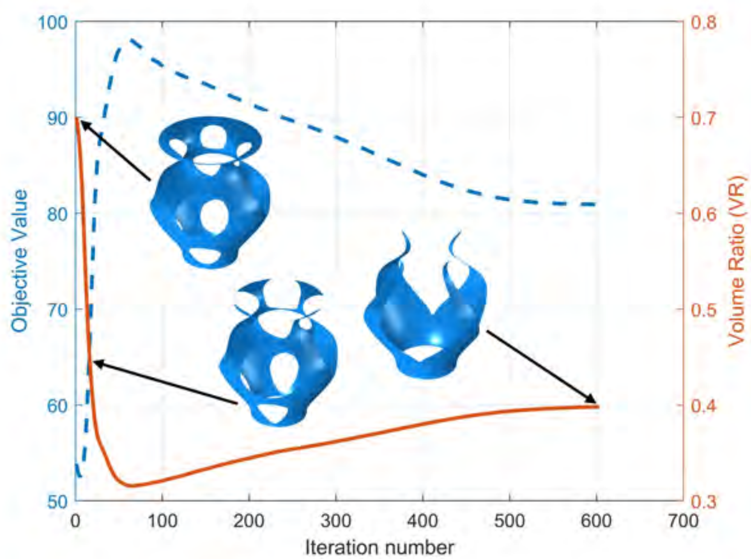

Figure 25: Convergence history of the vase example

surface in 3D space can now be equivalently transferred and solved on the 2D parameter domain. This is made possible by the fact that the covariant derivatives on the manifolds can be represented by the Euclidean gradient operators multiplied by a scalar with the conformal mapping. Resting on this relation, both the physics equation and the Hamilton-Jacobi equation, which govern the physics phenomena and the structural boundary evolution, can now be transformed and resolved equivalently on the 2D parameter domain. Moreover, the related physics quantities such as the objective function, current volume, and the normal velocity are also equivalently evaluated on the 2D parameter domain with a properly modified form. In this way, we convert the 3D topology

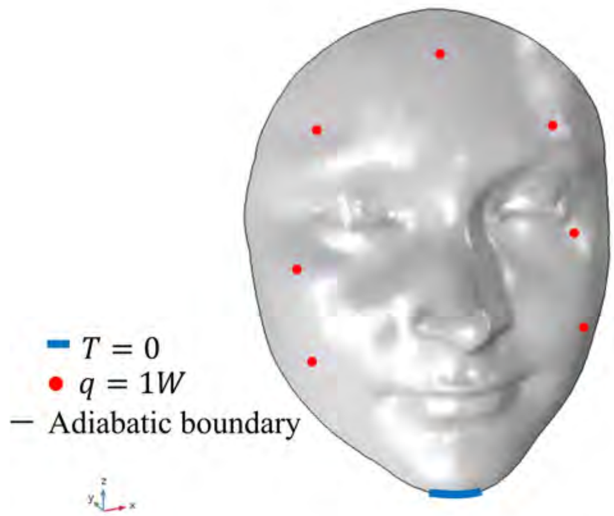

Figure 26: Boundary conditions of the human face with multiple nodal heat sources

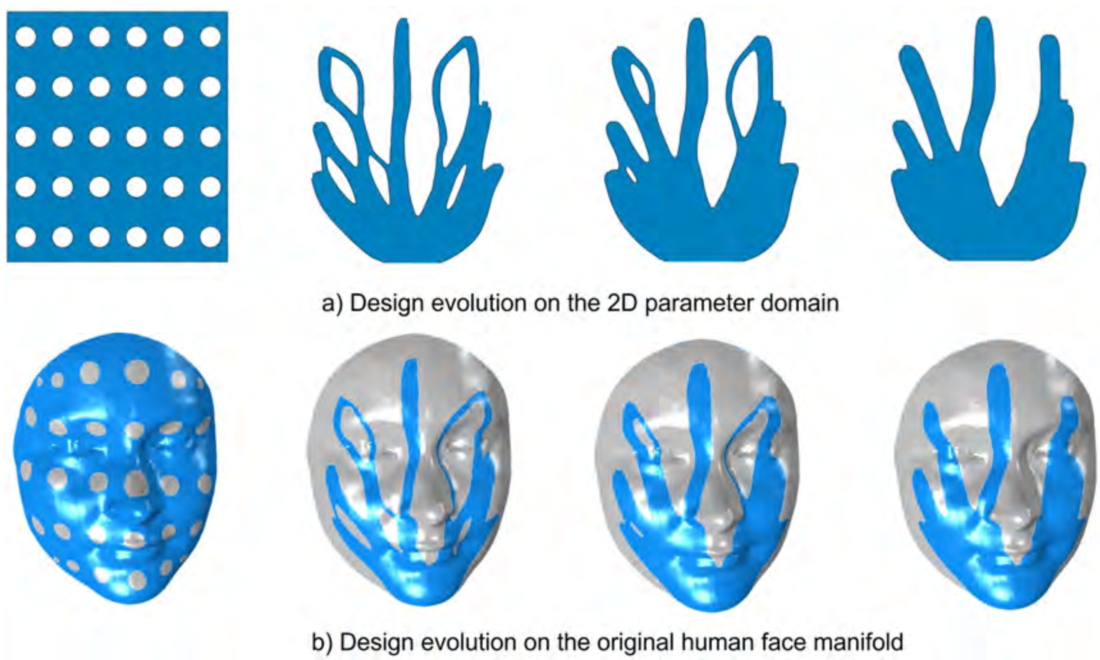

Figure 27: The design evolution of the human face example

optimization problem into a 2D problem.

By definition, a thin-shell structure is a shell with a thickness that is considerably small compared to its other dimensions. In contrast to the 3D solid models, the thin-shell models will be discretized with surface meshes, e.g., surface triangulation, for finite element analysis purpose. When we employ a thin-shell model or plate structure, it is assumed that there is no variation of the state variable in the thickness direction, although a specific thickness must be assigned to carry out the FEA. In the X-LSM and DR-LSM proposed in this paper, the free-form shell manifolds have a uniform thickness 0.01 for all the provided numerical examples. The same thickness 0.01

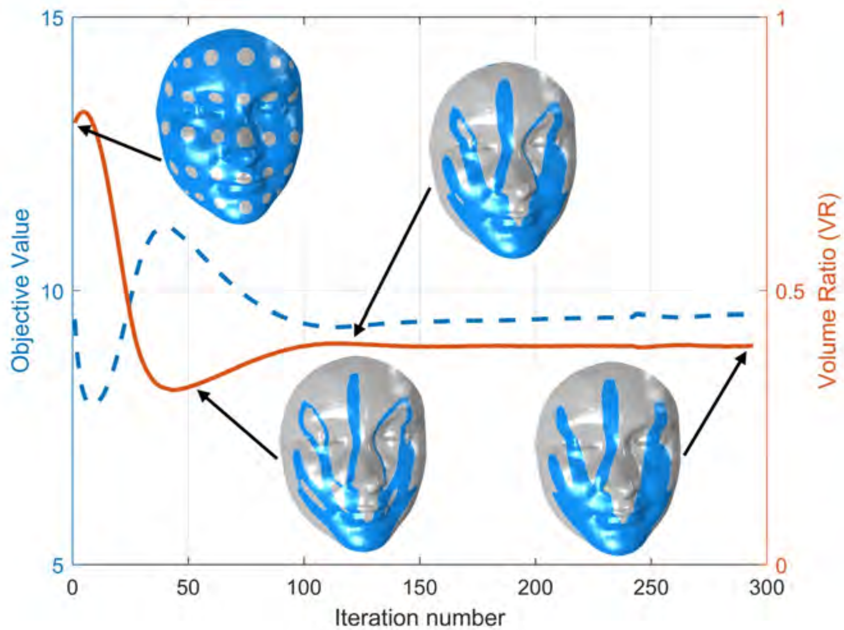

Figure 28: Convergence history of the human face example

is assigned to the 2D parameter rectangle domains obtained from the conformal parameterization. Although the thickness would have an impact on the final objective function value, i.e., thermal compliance in this study, it does not affect the final optimized structures in terms of shape and topology. According to our experience, the consistency will be guaranteed between the original optimization problems defined on the thin-shell manifolds in 3D space and the modified ones on the 2D parameter domains, as long as the same thickness value is applied to both 3D and 2D models. As a matter of fact, it is not advisable to assign a large thickness to the shell models, which might violate the various assumptions specifically made for the thin-shell structures. In that case, it would be more appropriate to treat it as a solid 3D model.

In this study, we apply the DR-LSM to solve a heat conduction topology optimization problem on the manifold. The feasibility and validity of this dimension reduction formulation from the proposed DR-LSM are demonstrated through the first three numerical examples (Section 6.1, 6.2 and 6.3) containing the comparisons with the conventional X-LSM. The final optimized designs obtained from the proposed DR-LSM and the conventional X-LSM are nearly identical, and the values of the objective functions show little difference. Moreover, the DR-LSM and the X-LSM use the same parameters for the augmented Lagrangian method to impose the volume constraints for each of the above three numerical examples. They share a close convergence history as shown in Figure 10, 15 and 20. One main benefit of this dimension reduction formulation is the reduction of computational costs. The average cost reduction by the DR-LSM in terms of the total computational time and time per iteration can reach 31.56% and 24.76%, respectively, for the aforementioned three numerical examples. Comparing the workflow of the DR-LSM in Figure 5 and the X-LSM in Figure 29, we can observe that the X-LSM employs two more interpolation processes. One is intended to interpolate the level set function from the 2D parameter domain to the manifold in 3D space, where the FEA is conducted. The other one is used to interpolate the normal

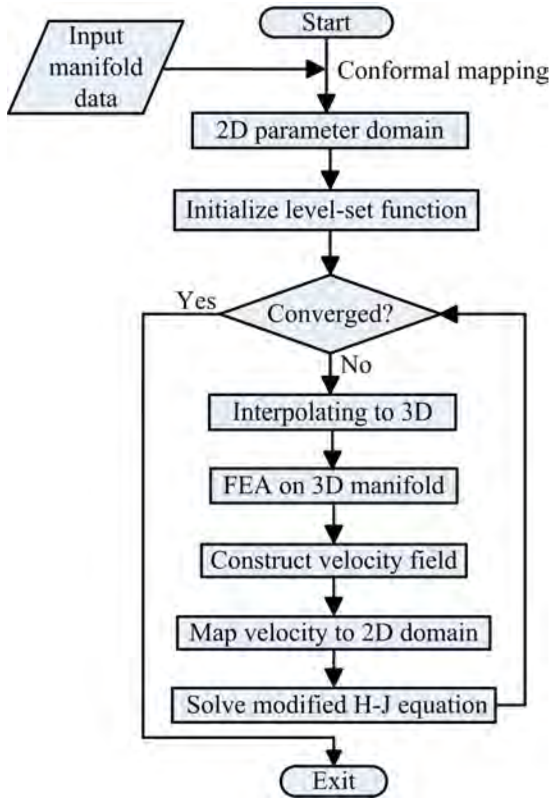

Figure 29: The flowchart of the X-LSM [14]

velocity field generated from the manifold back to the 2D parameter domain, where the modified Hamilton-Jacobi equation is solved to evolve the structural boundaries. The elimination of the two interpolation steps accounts for part of the computational savings induced by the DR-LSM. For the FEA process, the DR-LSM and X-LSM employ a similar number of triangular elements. For pure heat conduction topology optimization problems, the state variable is a scalar function, i.e., the temperature field T. The number of degree of freedom (DOF) does not change much when we reduce the dimension of the FEA from the manifold in 3D space to the 2D parameter domain. Nevertheless, the FEA process in the DR-LSM costs less time per iteration than the X-LSM as there will be a z component in the heat equation for the latter.

7.2. The extension to other physics problems

Analogous to the minimum compliance problems in linear elasticity, the pure heat conduction problems considered in this study are computationally friendly. They are self-adjoint in terms of the shape sensitivity analysis. In other words, we can directly write down the explicit expression for the normal velocity V_n in the level set framework. Under the conformal parameterization, the normal velocity V_n will have a properly modified form on the 2D parameter domain to solve the modified H-J equation. In most cases, however, the shape sensitivity analysis will come with an adjoint equation, which needs to be solved for the adjoint variables and further the normal velocity V_n. In such scenarios, we need to apply the conformal parameterization to the adjoint equation as well to be able to solve it on the 2D parameter domain equivalently. In short, we can solve the PDEs initially defined on manifolds equivalently on the 2D parameter domain with a properly modified form under the conformal parameterization.

The proposed DR-LSM can be easily extended to other physical problems when the state variable is a scalable function. Examples include electric conduction problems, magneto-statics problems, and electrostatics problems, to name a few. In this paper, we assume that all the material properties are isotropic. The physics property of interest is the thermal conductivity k, which will be a scalar for isotropic thermal materials. When the solid thermal material exhibits anisotropic thermal conductivity, the k in the heat equation will then be a tensor. For the original heat equation defined on the manifold in 3D space, the k will be a 3×3 tensor. When we apply the conformal parameterization to obtain the modified heat equation on the 2D domain, the k will become a 2×2 tensor. How the transition from a 3×3 tensor to a 2×2 one is specifically finished requires further investigation. Theoretically, it is achievable as an example of Navier-Stokes equation was reported in [42], which is originally defined on the manifold in 3D space and equivalently solved on the 2D parameter domain by applying the global conformal parameterization. Specifically, the original Navier-Stokes equation defined on a manifold M can be given as:

$$\frac{\partial \mathbf{u}}{\partial t} = -(\mathbf{u}\cdot\nabla_M)\mathbf{u} + v\Delta_M\mathbf{u} + \mathbf{f}, \tag{34}$$

where $\mathbf{u} = (u_1, u_2, u_3)$ is the fluid velocity, v is viscosity and $\mathbf{f} = (f_1, f_2, f_3)$ are the external forces. Suppose there is a conformal parameterization between the manifold M and the 2D domain S with a conformal factor $e^{2\lambda}$. Then the modified Navier-Stokes equation after conformal parameterization can be given as:

$$\frac{\partial \bar{\mathbf{u}}}{\partial t} = -e^{-2\lambda}(\bar{\mathbf{u}}\cdot\nabla)\bar{\mathbf{u}} + e^{-2\lambda}v\Delta\bar{\mathbf{u}} + \bar{\mathbf{f}}, \tag{35}$$

where $\bar{\mathbf{u}} = (\bar{u}_1, \bar{u}_2)$ is the fluid velocity, v is viscosity and $\bar{\mathbf{f}} = (\bar{f}_1, \bar{f}_2)$ are the external forces. In this case, how the original 3×1 $\mathbf{f}$ vector is reduced as a 2×1 $\bar{\mathbf{f}}$ is worth an in-depth investigation.

The Navier-Stokes equation discussed above is somehow intuitive as the fluid flow only happens on surface. By "on surface", it refers to the fact that the computed state variable $\mathbf{u}$ at any points on the manifold will be on its tangent plane, i.e., there will be no out-of-surface component. Physically, it means the fluid can not flow out of the manifold except from the boundaries. A further discussion can lead us to a more complex scenario, where the out-of-surface deformation can happen. A typical example is the minimum compliance problem in linear elasticity on thin-shell manifolds. In this scenario, the state variable will then be a displacement vector, which does not necessarily lie on the tangent plane at a certain point on the manifold. Physically, it means the out-of-surface deformation is allowed. On the 2D parameter domain, however, it is challenging to consider the out-of-plane deformation since it is assumed there is no z component of the displacement solution for a 2D planar model. In the future work, we will devote our efforts to figuring out how the anisotropy of the thermal conductivity can be taken into account and how to extend the DR-LSM to more complex physics problem with vector state variable fields, e.g., minimum compliance problem in linear elasticity with the aid of tensor calculus [87].

Acknowledgment

The authors gratefully acknowledge financial support from the National Science Foundation (CMMI-1762287), the Ford University Research Program (URP) (Award No. 2017-9198R), and the State University of New York (SUNY) at Stony Brook. The first author, Mr. Xiaoqiang Xu, would like to thank Dr. Yang Guo and Dr. Qian Ye for their insightful discussions on the formulations of this method.

References

[1] K. V. Wong, A. Hernandez, A review of additive manufacturing, International scholarly research notices 2012 (2012).

[2] W. E. Frazier, Metal additive manufacturing: a review, Journal of Materials Engineering and performance 23 (6) (2014) 1917–1928.

[3] D. Herzog, V. Seyda, E. Wycisk, C. Emmelmann, Additive manufacturing of metals, Acta Materialia 117 (2016) 371–392.

[4] T. Zegard, G. H. Paulino, Bridging topology optimization and additive manufacturing, Structural and Multidisciplinary Optimization 53 (1) (2016) 175–192.

[5] J. Liu, A. T. Gaynor, S. Chen, Z. Kang, K. Suresh, A. Takezawa, L. Li, J. Kato, J. Tang, C. C. Wang, et al., Current and future trends in topology optimization for additive manufacturing, Structural and Multidisciplinary Optimization 57 (6) (2018) 2457–2483.

[6] W. Zuo, K. Saitou, Multi-material topology optimization using ordered simp interpolation, Structural and Multidisciplinary Optimization 55 (2) (2017) 477–491.

[7] K. C. Nguyen, P. Tran, H. X. Nguyen, Multi-material topology optimization for additive manufacturing using polytree-based adaptive polygonal finite elements, Automation in Construction 99 (2019) 79–90.

[8] J. Tian, X. D. Gu, S. Chen, Multi-material topology optimization of ferromagnetic soft robots using reconciled level set method, in: International Design Engineering Technical Conferences and Computers and Information in Engineering Conference, Vol. 85451, American Society of Mechanical Engineers, 2021, p. V08BT08A014.

[9] X. Xu, Y. Wu, L. Zuo, S. Chen, Topology optimization of multimaterial thermoelectric structures, Journal of Mechanical Design 143 (1) (2021) 011705.

[10] X. Xu, Y. Wu, L. Zuo, S. Chen, Multimaterial topology optimization of thermoelectric generators, in: International Design Engineering Technical Conferences and Computers and Information in Engineering Conference, Vol. 59186, American Society of Mechanical Engineers, 2019, p. V02AT03A064.

[11] R. Sivapuram, P. D. Dunning, H. A. Kim, Simultaneous material and structural optimization by multiscale topology optimization, Structural and multidisciplinary optimization 54 (5) (2016) 1267–1281.

[12] L. Xia, P. Breitkopf, Recent advances on topology optimization of multiscale nonlinear structures, Archives of Computational Methods in Engineering 24 (2) (2017) 227–249.

[13] L. Jiang, Y. Guo, S. Chen, P. Wei, N. Lei, X. D. Gu, Concurrent optimization of structural topology and infill properties with a cbf-based level set method, Frontiers of Mechanical Engineering 14 (2) (2019) 171–189.

[14] Q. Ye, Y. Guo, S. Chen, N. Lei, X. D. Gu, Topology optimization of conformal structures on manifolds using extended level set methods (x-lsm) and conformal geometry theory, Computer Methods in Applied Mechanics and Engineering 344 (2019) 164–185.

[15] P. Vogiatzis, M. Ma, S. Chen, X. D. Gu, Computational design and additive manufacturing of periodic conformal metasurfaces by synthesizing topology optimization with conformal mapping, Computer Methods in Applied Mechanics and Engineering 328 (2018) 477–497.

[16] J. Nguyen, S.-I. Park, D. W. Rosen, L. Folgar, J. Williams, Conformal lattice structure design and fabrication, in: Solid freeform fabrication symposium, Austin, TX, 2012, pp. 138–161.

[17] E. Fauche, S. Adriaenssens, J. H. Prevost, Structural optimization of a thin-shell bridge structure, Journal of the International Association for Shell and Spatial Structures 51 (2) (2010) 153–160.

[18] S. Adriaenssens, P. Block, D. Veenendaal, C. Williams, Shell structures for architecture: form finding and optimization, Routledge, 2014.

[19] A. Nathan, A. Ahnood, M. T. Cole, S. Lee, Y. Suzuki, P. Hiralal, F. Bonaccorso, T. Hasan, L. Garcia-Gancedo, A. Dyadyusha, et al., Flexible electronics: the next ubiquitous platform, Proceedings of the IEEE 100 (Special Centennial Issue) (2012) 1486–1517.

[20] W. Gao, H. Ota, D. Kiriya, K. Takei, A. Javey, Flexible electronics toward wearable sensing, Accounts of chemical research 52 (3) (2019) 523–533.

[21] J.-H. Zhu, W.-H. Zhang, L. Xia, Topology optimization in aircraft and aerospace structures design, Archives of Computational Methods in Engineering 23 (4) (2016) 595–622.

[22] J. Stegmann, E. Lund, Discrete material optimization of general composite shell structures, International Journal for Numerical Methods in Engineering 62 (14) (2005) 2009–2027.

[23] E. Lund, J. Stegmann, On structural optimization of composite shell structures using a discrete constitutive parametrization, Wind Energy: An International Journal for Progress and Applications in Wind Power Conversion Technology 8 (1) (2005) 109–124.

[24] E. Lund, Buckling topology optimization of laminated multi-material composite shell structures, Composite Structures 91 (2) (2009) 158–167.

[25] M. P. Bendsøe, N. Kikuchi, Generating optimal topologies in structural design using a homogenization method, Computer methods in applied mechanics and engineering 71 (2) (1988) 197–224.

[26] M. P. Bendsøe, Optimal shape design as a material distribution problem, Structural optimization 1 (4) (1989) 193–202.

[27] M. Zhou, G. Rozvany, The coc algorithm, part ii: Topological, geometrical and generalized shape optimization, Computer methods in applied mechanics and engineering 89 (1-3) (1991) 309–336.

[28] K. Maute, E. Ramm, Adaptive topology optimization of shell structures, AIAA journal 35 (11) (1997) 1767–1773.

[29] R. Ansola, J. Canales, J. A. Tarrago, J. Rasmussen, An integrated approach for shape and topology optimization of shell structures, Computers & structures 80 (5-6) (2002) 449–458.

[30] R. Ansola, J. Canales, J. Tarrago, J. Rasmussen, Combined shape and reinforcement layout optimization of shell structures, Structural and Multidisciplinary Optimization 27 (4) (2004) 219–227.

[31] A. Clausen, E. Andreassen, O. Sigmund, Topology optimization of 3d shell structures with porous infill, Acta Mechanica Sinica 33 (4) (2017) 778–791.

[32] E. A. Träff, O. Sigmund, N. Aage, Topology optimization of ultra high resolution shell structures, Thin-Walled Structures 160 (2021) 107349.

[33] O. Sigmund, J. Petersson, Numerical instabilities in topology optimization: a survey on procedures dealing with checkerboards, mesh-dependencies and local minima, Structural optimization 16 (1) (1998) 68–75.

[34] B. S. Lazarov, O. Sigmund, Filters in topology optimization based on helmholtz-type differential equations, International Journal for Numerical Methods in Engineering 86 (6) (2011) 765–781.

[35] B. Bourdin, Filters in topology optimization, International journal for numerical methods in engineering 50 (9) (2001) 2143–2158.

[36] U. Clarenz, M. Rumpf, A. Telea, Surface processing methods for point sets using finite elements, Computers & Graphics 28 (6) (2004) 851–868.

[37] G. Dziuk, C. M. Elliott, Finite element methods for surface pdes, Acta Numerica 22 (2013) 289–396.

[38] L. M. Lui, X. Gu, T. F. Chan, S.-T. Yau, et al., Variational method on riemann surfaces using conformal parameterization and its applications to image processing, Methods and Applications of Analysis 15 (4) (2008) 513–538.

[39] A. Bartezzaghi, L. Dedè, A. Quarteroni, Isogeometric analysis of high order partial differential equations on surfaces, Computer Methods in Applied Mechanics and Engineering 295 (2015) 446–469.

[40] S. J. Ruuth, B. Merriman, A simple embedding method for solving partial differential equations on surfaces, Journal of Computational Physics 227 (3) (2008) 1943–1961.

[41] M. Bertalmıo, L.-T. Cheng, S. Osher, G. Sapiro, Variational problems and partial differential equations on implicit surfaces, Journal of Computational Physics 174 (2) (2001) 759–780.

[42] L. M. Lui, Y. Wang, T. F. Chan, Solving pdes on manifolds with global conformal parametriazation, in: International Workshop on Variational, Geometric, and Level Set Methods in Computer Vision, Springer, 2005, pp. 307–319.

[43] Q. Ye, Y. Guo, S. Chen, X. D. Gu, N. Lei, Topology optimization of conformal structures using extended level set methods and conformal geometry theory, in: International Design Engineering Technical Conferences and Computers and Information in Engineering Conference, Vol. 51760, American Society of Mechanical Engineers, 2018, p. V02BT03A038.

[44] X. D. Gu, S.-T. Yau, Computational conformal geometry, Vol. 1, International Press Somerville, MA, 2008.

[45] Y. M. Xie, G. P. Steven, A simple evolutionary procedure for structural optimization, Computers & structures 49 (5) (1993) 885–896.

[46] M. Y. Wang, X. Wang, D. Guo, A level set method for structural topology optimization, Computer methods in applied mechanics and engineering 192 (1-2) (2003) 227–246.

[47] G. Allaire, F. Jouve, A.-M. Toader, Structural optimization using sensitivity analysis and a level-set method, Journal of computational physics 194 (1) (2004) 363–393.

[48] X. Guo, W. Zhang, W. Zhong, Doing topology optimization explicitly and geometrically—a new moving morphable components based framework, Journal of Applied Mechanics 81 (8) (2014).

[49] W. Zhang, J. Yuan, J. Zhang, X. Guo, A new topology optimization approach based on moving morphable components (mmc) and the ersatz material model, Structural and Multidisciplinary Optimization 53 (6) (2016) 1243–1260.

[50] J. Norato, B. Bell, D. A. Tortorelli, A geometry projection method for continuum-based topology optimization with discrete elements, Computer Methods in Applied Mechanics and Engineering 293 (2015) 306–327.

[51] X. Xu, S. Chen, X. D. Gu, M. Y. Wang, Conformal topology optimization of heat conduction problems on manifolds using an extended level set method (x-lsm), in: International Design Engineering Technical Conferences and Computers and Information in Engineering Conference, Vol. 85390, American Society of Mechanical Engineers, 2021, p. V03BT03A030.

[52] Q. Ye, L. Jiang, S. Chen, X. Gu, Generative design of multifunctional conformal structures using extended level set methods (x-lsm) and conformal geometry theory, in: IUTAM Symposium on When topology optimization meets additive manufacturing-theory and methods, 2018.

[53] J. Tian, X. Zhao, X. D. Gu, S. Chen, Designing ferromagnetic soft robots (ferrosoro) with level-set-based multiphysics topology optimization, in: 2020 IEEE International Conference on Robotics and Automation (ICRA), IEEE, 2020, pp. 10067–10074.

[54] J. Tian, X. Zhao, X. D. Gu, S. Chen, Designing conformal ferromagnetic soft actuators using extended level set methods (x-lsm), in: International Design Engineering Technical Conferences and Computers and Information in Engineering Conference, Vol. 83990, American Society of Mechanical Engineers, 2020, p. V010T10A012.

[55] J. Tian, M. Li, Z. Han, Y. Chen, X. D. Gu, Q. Ge, S. Chen, Conformal topology optimization of multi-material ferromagnetic soft active structures using an extended level set method, Computer Methods in Applied Mechanics and Engineering 389 (2022) 114394.

[56] K.-S. Park, S.-K. Youn, Topology optimization of shell structures using adaptive inner-front (aif) level set method, Structural and Multidisciplinary Optimization 36 (1) (2008) 43–58.

[57] J. Graef, R. Shivaji, B. Soni, J. Zhu, Governing equations of fluid mechanics in physical curvilinear coordinate system, in: Differential Equations and Computational Simulations, Conference, Vol. 1, 1997, pp. 149–157.

[58] T. Ho-Nguyen-Tan, H.-G. Kim, Level set-based topology optimization for compliance and stress minimization of shell structures using trimmed quadrilateral shell meshes, Computers & Structures 259 (2022) 106695.

[59] T. H. Nguyen, G. H. Paulino, J. Song, C. H. Le, A computational paradigm for multiresolution topology optimization (mtop), Structural and Multidisciplinary Optimization 41 (4) (2010) 525–539.

[60] T. Dbouk, A review about the engineering design of optimal heat transfer systems using topology optimization, Applied Thermal Engineering 112 (2017) 841–854.

[61] E. M. Dede, Multiphysics topology optimization of heat transfer and fluid flow systems, in: proceedings of the COMSOL Users Conference, 2009.

[62] S. Sun, P. Liebersbach, X. Qian, 3d topology optimization of heat sinks for liquid cooling, Applied Thermal Engineering 178 (2020) 115540.

[63] T. Lei, J. Alexandersen, B. S. Lazarov, F. Wang, J. H. Haertel, S. De Angelis, S. Sanna, O. Sigmund, K. Engelbrecht, Investment casting and experimental testing of heat sinks designed by topology optimization, International Journal of Heat and Mass Transfer 127 (2018) 396–412.

[64] J. Alexandersen, O. Sigmund, N. Aage, Large scale three-dimensional topology optimisation of heat sinks cooled by natural convection, International Journal of Heat and Mass Transfer 100 (2016) 876–891.

[65] A. Donoso, P. Pedregal, Optimal design of 2d conducting graded materials by minimizing quadratic functionals in the field, Structural and Multidisciplinary Optimization 30 (5) (2005) 360–367.

[66] F. H. Burger, J. Dirker, J. P. Meyer, Three-dimensional conductive heat transfer topology optimisation in a cubic domain for the volume-to-surface problem, International Journal of Heat and Mass Transfer 67 (2013) 214–224.

[67] Y. Zhang, H. Qiao, S. Liu, Design of the heat conduction structure based on the topology optimization, INTECH Open Access Publisher, 2011.

[68] T. E. Bruns, Topology optimization of convection-dominated, steady-state heat transfer problems, International Journal of Heat and Mass Transfer 50 (15-16) (2007) 2859–2873.

[69] B. Zhu, X. Zhang, N. Wang, S. Fatikow, Optimize heat conduction problem using level set method with a weighting based velocity constructing scheme, International Journal of Heat and Mass Transfer 99 (2016) 441–451.

[70] B. S. Lazarov, J. Alexandersen, O. Sigmund, Topology optimized designs of steady state conduction heat transfer problems with convection boundary conditions, EngOpt (2014).

[71] A. Iga, S. Nishiwaki, K. Izui, M. Yoshimura, Topology optimization for thermal conductors considering design-dependent effects, including heat conduction and convection, International Journal of Heat and Mass Transfer 52 (11-12) (2009) 2721–2732.

[72] A. Gersborg-Hansen, M. P. Bendsøe, O. Sigmund, Topology optimization of heat conduction problems using the finite volume method, Structural and multidisciplinary optimization 31 (4) (2006) 251–259.

[73] Q. Li, G. P. Steven, Y. M. Xie, O. M. Querin, Evolutionary topology optimization for temperature reduction of heat conducting fields, International Journal of Heat and Mass Transfer 47 (23) (2004) 5071–5083.

[74] C. Zhuang, Z. Xiong, H. Ding, A level set method for topology optimization of heat conduction problem under multiple load cases, Computer methods in applied mechanics and engineering 196 (4-6) (2007) 1074–1084.

[75] Q. Xia, T. Shi, L. Xia, Topology optimization for heat conduction by combining level set method and beso method, International Journal of Heat and Mass Transfer 127 (2018) 200–209.

[76] T. Yamada, K. Izui, S. Nishiwaki, A level set-based topology optimization method for maximizing thermal diffusivity in problems including design-dependent effects, Journal of Mechanical Design 133 (3) (2011).

[77] J. A. Sethian, A. Wiegmann, Structural boundary design via level set and immersed interface methods, Journal of computational physics 163 (2) (2000) 489–528.

[78] S. Osher, R. Fedkiw, K. Piechor, Level set methods and dynamic implicit surfaces, Appl. Mech. Rev. 57 (3) (2004) B15–B15.

[79] K. Crane, U. Pinkall, P. Schröder, Spin transformations of discrete surfaces, in: ACM SIGGRAPH 2011 papers, 2011, pp. 1–10.

[80] R. S. Hamilton, The ricci flow on surfaces, in: Mathematics and general relativity, Proceedings of the AMS-IMS-SIAM Joint Summer Research Conference in the Mathematical Sciences on Mathematics in General Relativity, Univ. of California, Santa Cruz, California, 1986, Amer. Math. Soc., 1988, pp. 237–262.

[81] W. Zeng, X. D. Gu, Ricci flow for shape analysis and surface registration: theories, algorithms and applications, Springer Science & Business Media, 2013.

[82] K. K. Choi, N.-H. Kim, Structural sensitivity analysis and optimization 1: linear systems, Springer Science & Business Media, 2004.

[83] G. Allaire, A review of adjoint methods for sensitivity analysis, uncertainty quantification and optimization in numerical codes, Ingénieurs de l'Automobile 836 (2015) 33–36.

[84] Q. Xia, M. Y. Wang, Topology optimization of thermoelastic structures using level set method, Computational Mechanics 42 (6) (2008) 837–857.

[85] N. Jorge, J. W. Stephen, Numerical optimization, Spinger, 2006.

[86] O. Al-Ketan, R. K. Abu Al-Rub, Multifunctional mechanical metamaterials based on triply periodic minimal surface lattices, Advanced Engineering Materials 21 (10) (2019) 1900524.

[87] J. L. Synge, A. Schild, Tensor calculus, University of Toronto Press, 2020.